ON THE USE OF SMOOTHED PARTICLE HYDRODYNAMICS TO MODEL ORTHOGONAL MACHINING

by

Chinmay Satish Avachat

A thesis submitted to the faculty of
The University of North Carolina at Charlotte
in partial fulfillment of the requirements
for the degree of Master of Science in
Mechanical Engineering

Charlotte

2014

Approved by:

_____
Dr. Harish P. Cherukuri

_____
Dr. Alireza Tabarraei

_____
Dr. Vincent (Tobi) Ogunro

ABSTRACT

CHINMAY SATISH AVACHAT. On the use of smoothed particle hydrodynamics to model orthogonal machining.
(Under the direction of DR. HARISH P. CHERUKURI)

Modeling machining processes with conventional finite element methods (FEM) is challenging due to the severe deformations that occur during machining, complex frictional conditions that exist between the cutting tool and the workpiece, and the possibility of self contact due to chip curling. Recently, the Smoothed Particle Hydrodynamics (SPH) method has emerged as a potential alternative for modeling machining processes due to its ability to handle severe deformations while avoiding mass and energy losses encountered by traditional FEM. The method has been implemented in several commercial finite element packages such as `ABAQUS` and `LS-DYNA` for solving problems involving localized severe deformations.

The SPH method belongs to a class of numerical methods collectively known as meshless or mesh-free methods. In the SPH method, the given domain is discretized into a set of particles and the properties and field variables associated with each particle are obtained by taking into account the particles within its neighborhood defined by a smoothing length and a kernel function. The method employs several parameters for controlling the particle behavior during deformations and the accuracy of the solution depends on an optimal combination of these parameters. The three most important parameters are, the smoothing length, particle density, and the type of SPH formulation. In the present work, the effects of these parameters on the chip morphology, stress distribution and cutting force in the context of orthogonal machining of `AISI 1045` steel are investigated. The `LS-DYNA` finite element package along with Johnson-Cook material model is used for this purpose. Results from the parametric study are presented and the accuracy of the solutions as compared with

the results from conventional FEM are discussed. In addition, five different sets of values available in the literature are considered for the Johnson-Cook material model for `AISI 1045` steel. The sensitivity of chip morphology and stress distribution on these material parameters is discussed.

DEDICATION

With utmost happiness, I would like to dedicate my master's thesis to my loving parents, Satish Vasant Avachat and Ruchita Satish Avachat, and to all my teachers and friends for imparting endless knowledge, love, support and encouragement.

ACKNOWLEDGMENTS

I would like to thank my advisor Dr. Harish P. Cherukuri for inspiring me to achieve this level of success in my master's thesis. His helpfulness, encouragement and patience helped in bringing out the best of my abilities.

I would like to thank my co-advisor Dr. Alireza Tabarraei for the valuable inputs during group meetings and his encouragement in the present work.

My advisors made my graduate studies at UNC Charlotte an inspirational, fun and memorable experience.

I would like to thank Dr. Vincent (Tobi) Ogunro for graciously accepting to be part of my thesis committee.

I would also like to thank my parents and family for just about everything that makes me what I am today.

Finally, I would like to thank each member of my research group whose constructive critique helped me root out all the flaws and make this work more presentable.

TABLE OF CONTENTS

LIST OF FIGURES

LIST OF TABLES

CHAPTER 1: INTRODUCTION

1.1 Research Background

Machining is one of the most widely used processes in the component manufacturing industry. It is a process in which a raw material is cut into the required shape and size by a controlled material-removal process. In order to have increased control over the surface finish, dimensions of the product, power consumption by the machine tool and tool life, it is important to understand the machining process.

Modeling and simulations of machining have been carried out extensively to predict the behavior of various materials under various cutting conditions such as cutting speed, depth of cut and various tool dimensions. Two of the most commonly used methods for machining are the finite element method (FEM) and mesh-free methods. FEM has been the most preferred method to model machining until recently. It can simulate large deformations, effects of high strain rate, friction, contact and various other phenomena related to machining. The finite element based machining models use one of the three formulations: Lagrangian, Eulerian and Arbitrary Lagrangian-Eulerian (ALE). However, simulation of machining by FEM has disadvantages such as distortion of elements, fracture has to be defined as well as mass loss due to element deletion which also limits the prediction of cutting forces, residual stresses, strain and strain-rate. In recent times, mesh-free methods, namely Smoothed Particle Hydrodynamics (SPH) and Discrete Element Method (DEM) have been proposed to overcome the difficulties in modeling machining. Out of the two methods, the SPH method looks to be more promising.

The SPH Method belongs to the class of numerical methods collectively known as meshless or mesh-free methods. These methods have become popular due to their ability to handle severe deformations while avoiding mass and energy losses encountered by traditional finite element methods. In the SPH method, the given domain is discretized into a set of particles and the material properties and the field variables are assigned to each of these particles. The method has been implemented in many commercial finite element packages such as `LS-Dyna` [1] and `ABAQUS` [2].

1.2 Thesis Objective

The objective of this research was to model the orthogonal machining of `AISI 1045` steel with the Smoothed Particle Hydrodynamics (SPH) method and to study the suitability and reliability of the method for modeling machining. The numerical simulations were carried out using the commercial finite element package `LS-DYNA`. The geometry and boundary conditions are chosen consistent with the SPH models considered in the published literature. The Johnson-Cook constitutive material model is used to define the material properties. The obtained results are compared to previously obtained results from experiments as well as numerical studies. The effect of various SPH control parameters such as the smoothing length, particle density and type of SPH formulation and their effects on the field variables, chip morphology and computation time are studied. Additionally, other important SPH control parameters such as the use of artificial bulk viscosity, the scale factor for computed time-step and their effects on the results are also discussed. Numerical simulations were also carried out for various Johnson-Cook parameters found in the published literature for `AISI 1045` steel and the effect that the variations in these parameters have on the chip morphology and field variables is evaluated. Furthermore, the effect of varying the machining parameters such as the depth of cut and cutting speed are also discussed.

CHAPTER 2: LITERATURE REVIEW

The SPH Method belongs to the class of numerical methods collectively known as meshless or mesh-free methods. The SPH method has the ability to handle severe deformations while avoiding mass and energy losses. In the recent years, there has been an increased interest amongst many researchers to model the machining process by the SPH method due to its many merits.

With the aim to study how the SPH method can be used to model machining, an overview about the machining process and the previous studies that have been conducted to model the machining process are discussed below.

Over a 100 years ago, Tresca (1878) visualized the visco-plasticity of the metal cutting process. He gave an opinion that for the construction of the best form of tools and for determining the most suitable depth of cut (or undeformed chip thickness), the minute examination of the cuttings is of the greatest importance [3].

2.1 Mechanics of Chip Formation

2.1.1 Types of Cutting Operations

Generally, the three cutting operations that are used are turning, milling and drilling [3]. In this process a single point tool is used to remove unwanted material. The cutting tool is fed towards a rotating workpiece to create an internal or external surface that is concentric with the axis of rotation. The lathe machine, which is one of the oldest and most versatile machine tools is used to carry out turning operations. In this thesis, we mainly concentrate on orthogonal cutting which is a variant of turning.

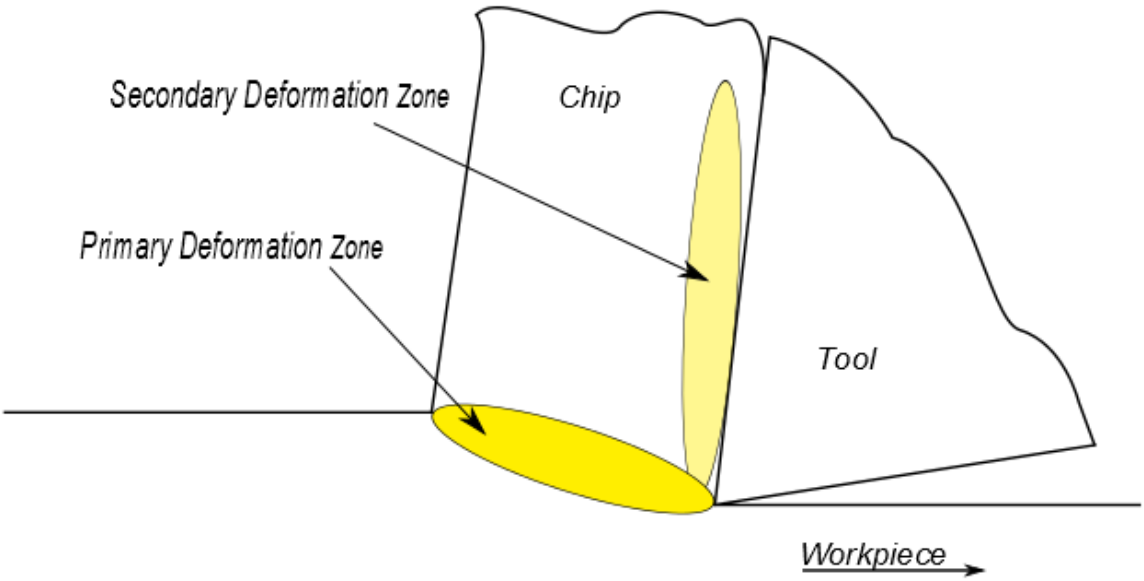

Figure 2.1: Deformation zones during the machining process.

2.1.2 Orthogonal Cutting

The turning process is further classified into orthogonal cutting and oblique cutting. This classification is based on the way the tool makes contact with the workpiece. Orthogonal cutting relates to the case when the tool is set perpendicular to the direction of relative motion of the tool and the workpiece and thus, generates a surface that is parallel to the original plane surface of the material being cut. If the tool is not set perpendicular to the direction of relative motion of the tool and workpiece the this case is known as oblique cutting. Conventionally, the orthogonal and oblique cutting processes are considered as two-dimensional and three-dimensional problems, respectively [3].

2.1.3 Deformation in the Workpiece

During metal cutting, three deformation zones are generally observed, which are, the Primary Deformation Zone, the Secondary Deformation Zone and the Tertiary Deformation Zone (a.k.a the machined surface) (See Figure 2.1). The primary deformation zone is formed when the material directly in front of the tool tip undergoes heavy plastic deformation and shearing as the tool penetrates and advances through

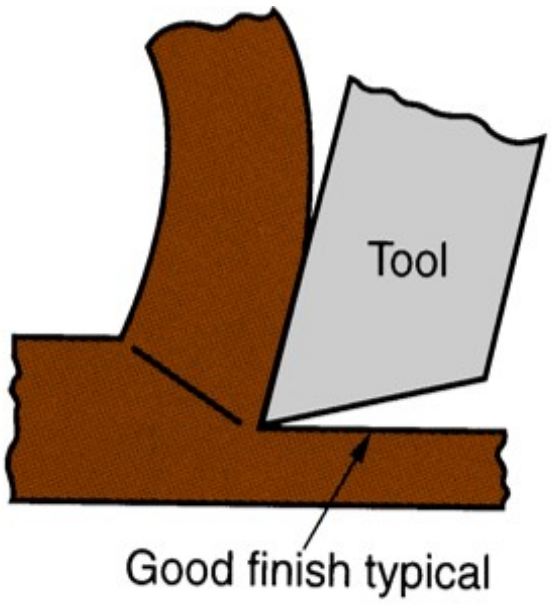

Figure 2.2: Continuous chip [8].

the workpiece. According to early literature [4–6] it was assumed that workpiece shearing occurs along a fixed primary shear plane which passes through the primary shear zone. The shear angle φ shown in fig, is the angle between the primary shear plane and the cutting direction. As the chip formed at the tool tip slides against the rake face of the tool, further deformation occurs due to friction between the two surfaces, which results in the formation of the secondary deformation zone. Lastly, the tertiary deformation zone is formed by the friction between the flank of the tool and the newly machined surface.

2.1.4 Classification of Chip Formation

During orthogonal cutting, the unwanted material removed is generally classified into four main categories [7].

Continuous Chip

Continuous chips are long ribbon-like chips, produced during the machining of ductile and soft materials such as mild steel, copper or aluminum, see Figure 2.2. They are generally formed at high cutting speed, low depth of cut and small feeds.

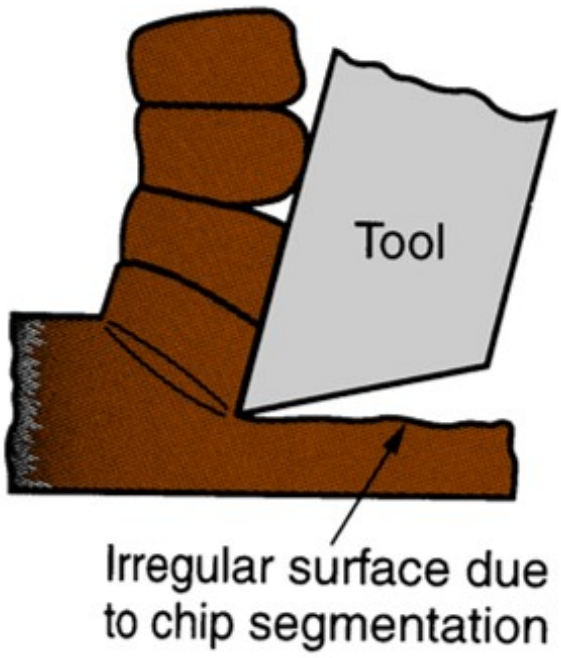

Figure 2.3: Discontinuous chip [8].

Continuous chips are an ideal type of chip for analysis as they are relatively simple to analyze and stable.

Discontinuous Chip

Segmented or discontinuous chips are formed during the machining of brittle materials such as cast iron or bronze, due to rupture occurring as the material cannot undergo high plastic deformation, see Figure 2.3. They are generally formed due to high tool-chip friction or at low cutting speeds, and also due to the large depth of cut.

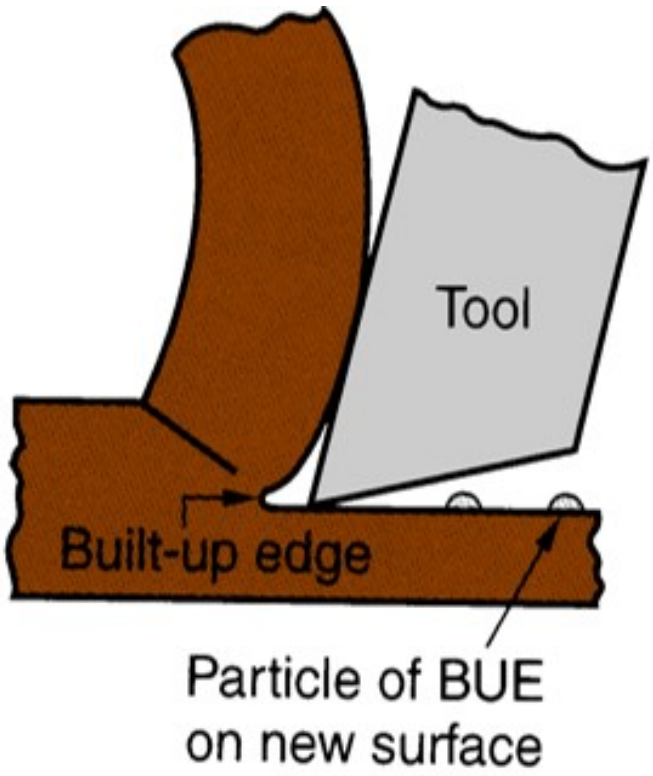

Figure 2.4: Continuous chip with built-up edge [8].

Continuous Chip with Built-up Edge

During the machining of ductile materials at low cutting speeds, when the temperature at the tool-chip interface is not very high, the chip can undergo a fracture in a plane perpendicular to the shear plane and thus, leaving behind a piece that attaches itself to the tool face. This attached portion now acts as the cutting edge and is known as the built-up edge (BUE), see Figure 2.4. This results in a change of the tool geometry and create imperfections in the machined surface. The undesirable formation of built-up edge can be corrected by the use of tools with a positive rake angle, by increasing the cutting speed or by the use of a coolant.

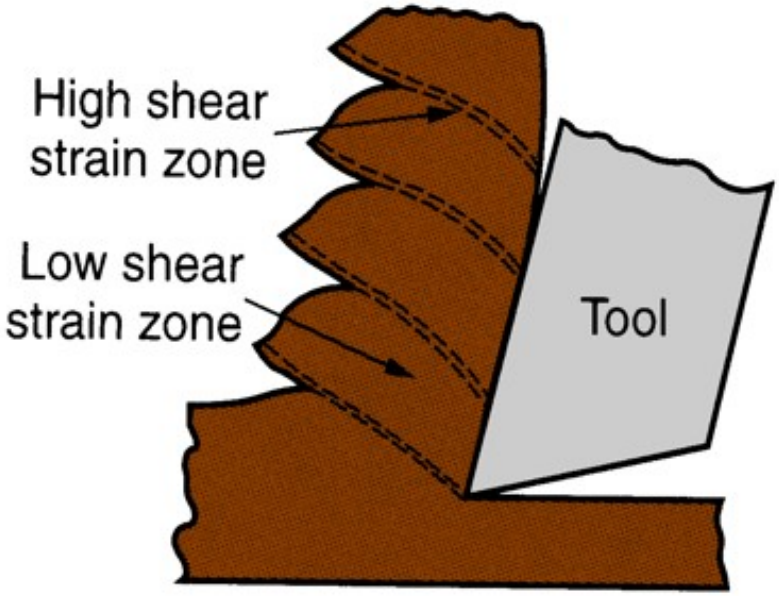

Figure 2.5: Serrated chip [8].

Serrated Chip

Thermoplastic instability which causes the formation of adiabatic shear bands or shear localization results in the formation of Saw-toothed or serrated chips [9], see Figure 2.5. In the primary shear zone the thermal softening occurs due to adiabatic plastic deformation. This thermal softening overrules the adiabatic or catastrophic shear band. This type of chip can be observed during the machining of stainless and hardened steels and titanium alloys at high cutting speeds.

2.2 Cutting Geometry, Stresses and Forces During the Orthogonal Cutting Process

A simplified two-dimensional model of the oblique cutting process (Orthogonal cutting) was given by Dr. Merchant in 1944 [4, 10]. Assuming that the force between the tool face and chip and also the workpiece and chip along the shear plane are equal in the equilibrium conditions and thus, these relationships were shown based on the force diagram (see Figure 2.6) as follows [4, 11]:

$$F_s = F_c cos\varphi - F_t sin\varphi, \tag{2.1}$$

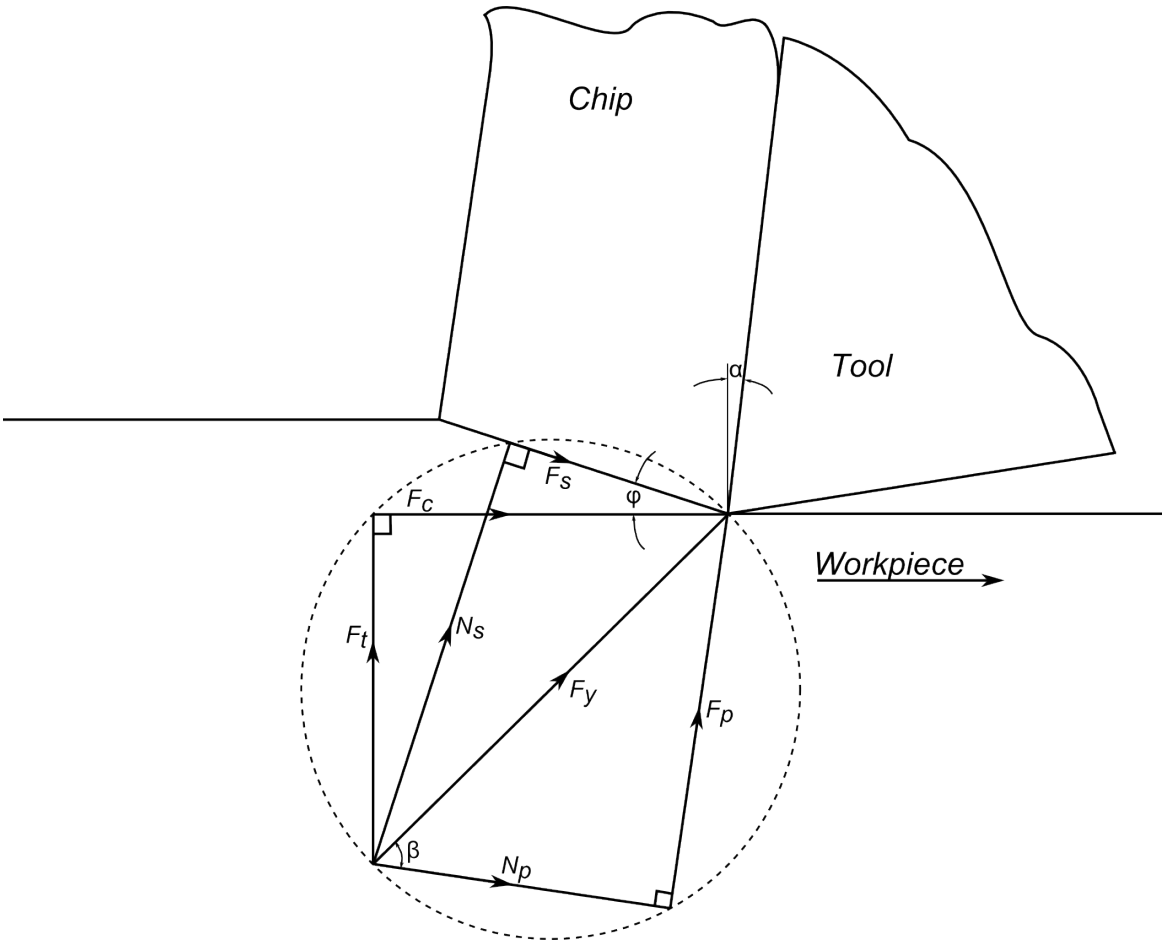

Figure 2.6: Force diagram.

$$N_s = F_c sin\varphi + F_t cos\varphi, \tag{2.2}$$

$$F_p = F_c sin\alpha + F_t cos\alpha, \tag{2.3}$$

$$N_p = F_c cos\alpha - F_t sin\alpha. \tag{2.4}$$

Here, φ is the shear angle, α is the rake angle of the tool, F_c is the cutting force, F_t is the thrust force, F_s is the shear force, N_s is the normal force on the shear plane, F_p is the shear force on the tool rake face and N_p is the normal force on the tool rake face.

To find the coefficient of friction on the tool face (μ), the components of the forces on the tool rake face are used as,

$$\mu = \frac{F_p}{N_p} = \frac{F_c sin\alpha + F_t cos\alpha}{F_c cos\alpha - F_t sin\alpha},$$

$$\mu = \frac{F_t + F_c tan\alpha}{F_c - F_t tan\alpha}. \tag{2.5}$$

To predict the stresses on the rake face and shear plane during orthogonal cutting, the card model or shear model proves to be simple and useful. The distribution of normal and shear forces on the tool rake face and shear plane are assumed to be uniform. Thus, the shear stress on the shear plane τ_s is found to be [11],

$$\tau_s = \frac{\text{Normal Force on shear plane}}{\text{Area of shear plane}},$$

$$\tau_s = \frac{F_c cos\varphi - F_t sin\varphi}{[\frac{w.f}{sin\varphi}]} \tag{2.6}$$

where, w is the depth of cut and f is the uncut chip thickness and is equal to the feed rate.

Now, σ_s i.e., the normal stress on the shear plane is calculated as,

$$\sigma_s = \frac{\text{Normal force on shear plane}}{\text{Area of shear plane}},$$

$$\sigma_s = \frac{F_c sin\varphi + F_t cos\varphi}{[\frac{w.f}{sin\varphi}]}. \tag{2.7}$$

In the same way, τ_f i.e., the shear stress on the rake face due to chip contact is calculated as,

$$\tau_f = \frac{F_c sin\alpha + N_s cos\alpha}{[w.l]} \tag{2.8}$$

and, σ_f i.e., the normal stress on the rake face is calculated as,

$$\sigma_f = \frac{F_c cos\alpha - N_s sin\alpha}{[w.l]}. \tag{2.9}$$

2.3 Previous Research in Modeling Orthogonal Cutting

Even though orthogonal machining is rarely used in practice, the method proves to be simple and important in scientific numerical studies. Finite element modeling of orthogonal machining began in the early 90's.

There are three vital parameters that are to be defined in an FEA model as they play an important role in the simulation. These are:

- Constitutive model: Defines the behavior of the material during cutting.
- Chip separation/fracture criteria: Controls the formation of the chip.
- Contact model: Governs the interaction of the tool-workpiece and tool-chip interface.

Klamecki and Kim [12], used a 3-D orthogonal machining model to study the effects of change in deformation state across the shear zone. They considered two cases which included one that assumed isothermal material deformation an another which took into effect the heat generation from deformation. Their results show varied magnitude, but constant equivalent strain contours with the two cases. The research showed that the dissipation of plastic energy with changes in stress states can cause large differences in deformation behavior. The actual transition in stress states was described by the variation of temperature found across the extreme plane strain and plane stress states. The fact that the work material in the plane strain region may be strain hardened and the material in the plane stress region may be thermally softened is because of the temperature variation in the shear zone.

Carrol, T. John and Strenkowski [13] at the Lawrence Livermore laboratory, produced two models of orthogonal machining using finite element analysis. In their

first model, they used the NIKE2D, which was an updated version of the large scale deformation Lagrangian code, to predict the cutting forces during the machining of Aluminum 2024-T361 by a single point diamond tool. In their second model, they modeled the workpiece as a rigid-viscoplastic material which had an Eulerian flow field close to the tool-workpiece interface. The chip separation/fracture criteria were based on the total effective strain for the Lagrangian formulation, where the workpiece was modeled as an elastic-plastic material. In order to neglect the thermal effects, the simulations were run at lower cutting speeds. The rake angles were in the range of -20° to 30°. The results faired well when compared with the experimental and analytical results published previously.

Shin, Chandrasekar and Yang [14] were able to produce a continuous chip with strain rate and temperature effects during the finite element simulation of orthogonal machining. The workpiece was modeled as a 1020 Carbon Steel and was simulated with the plane strain condition and a chip separation/damage criteria relative to the distance between the nodal point at the junction of the two elements ahead of the cutting tool and the tool tip. In order to improve the efficiency and accuracy of the computations a global and local mesh refining technique was used. The feed force and cutting force from simulated results agreed with the experimental results with respect to magnitude. This simulation also had the ability to show temperature distributions in addition to the stresses and strains at various points during the machining process.

Komvopoulos and Penderecki [15] developed a plane strain quasi static finite element simulation of orthogonal machining. The study was conducted with a ceramic coated tool on an AISI 4340 workpiece considering elastic-perfectly plastic and elastic-plastic with isotropic hardening. The model accounted for tool tip contact sliding friction, crater wear and built-up edge formation at the tool tip. Thinning of the primary shear zone was observed with the formation of a secondary shear zone due to the increased coefficient of friction. Distortion of the stress field at the interface,

a thinner chip and higher magnitude of cutting forces was observed with the simulations of the tool with a crater. When a friction coefficient of 0.5 and an elastic-plastic material model with isotropic hardening was used, the simulated results agreed with the experimental results.

Zhang and Bagchi [16] used a 2 node link element to define the separation criteria and simulated the chip formation during orthogonal machining. The tool was made of OHFC copper and the workpiece of 70/30 brass having a true stress-strain curve ranging from 0 to 3. The chip-tool contact was defined by a sticking and sliding friction model where the shear strength of the workpiece material was used for the sticking region and a constant friction model was employed in the sliding region. The results consisting of simulations using tools with different rake angles had up to 80% agreement with the experimental results which was good considering the approximations and assumptions. When a high cutting speed of 150-230 m/s was used the predicted cutting forces were very close to the experimental values.

Marusich and Ortiz [17] by accounting for the role of friction and thermal softening developed a successful finite element model on the machining of AISI 4340 steel. To simulate the formation of a discontinuous chip a new separation/fracture criteria based on void growth and coalescence in addition to the numerical methods for propagating and nucleating the crack through the deformed chip in a ductile material was developed. Other important aspects considered include thermal conductance, rate dependent plasticity, fracture and mechanical hardening with continuous meshing and remeshing. The simulations were successful in reproducing physical phenomena such as, increase of temperature distribution and cutting forces with increased feed, decrease of cutting force with an increase in tool rake angles and also had similar chip morphologies to that of experimental observations. The authors also stated that the results produced by the analytical method gave an approximate estimate as it does not consider the effects of thermal softening and thus concluded that their FEA

results gave a more accurate prediction.

A study to understand the different chip separation criteria used in the finite element machining models was carried out by Huang and Black [18]. There were four chip separation criteria consisting of one which was based on the distance between the tool tip and the node just ahead of the tool tip, a second which was based on the maximum shear stress in the element just ahead of the tool tip, a third which considered the distance as well as stress and lastly, a fourth based on the average maximum shear stress in the shear plane. It was concluded that during the steady state machining the choice of chip separation criteria did not influence neither the stress-strain distributions, nor the chip formation. Also, it was observed that none of the chip separation criteria accurately predict an initial stage of chip formation and thus, to learn about the initial stages of chip formation and also the steady state, a fusion of geometrical and physical criteria is to be developed. If only the steady state in machining is to be studied, then a geometrical criterion is sufficient.

Deshayes et al. [19] presented an experimental study of chip formation with validation using finite element simulations using `ABAQUS` and `ADVANTEDGE`, and also developed a classification of serrated chip morphology. This was achieved using the "fragmentation diagram which represents valid ranges for feed and depth of cut for a given combination of tool and workpiece material" [19, 20]. The authors concluded that with appropriate material models (Johnson-Cook) serrated chip formation can be simulated. Experimental observations show crack formation in the damaged region. Further work is needed to fully capture all parameters.

Buckkremer, Klocke and Lung [21] presented an analytical model of the equivalent plastic strain fields on free surface of chips and the effect of various parameters such as depth of cut, feed, cutting angle etc. on the equivalent strain fields. They used the visco-plastic material behavior described by a modified version of constitutive equations by Bai and Wierzbicki (BW model) [22]. They incorporated the influences

of stress triaxiality and Lode angle on the flow stress and final fracture strain. The authors concluded that chip breakage is a major machinability criterion in automated manufacturing. Chip breakage initiates after the equivalent strain on the chip free surface exceeds a limit. Knowledge of how the process conditions and thus, the chip geometry affects strain, is limited. A model of equivalent strain on the chip free surface considering chip geometry was proposed.

Agrawal and Joshi [23] developed an analytical model for the prediction of residual stresses in machining, considering the stress distribution in various cutting regions and also validated simulation results with the experimental data. From this study, the authors showed the influence of cutting tool edge radius, cutting speed, depth of cut and temperature on the residual stresses. A comparison was made with previous literature (S-J and Hybrid model [23]). The authors concluded that the residual stresses are tensile on the machined surface and compressive beneath the machined surface.

Arrazola et al. [24] conducted a new set of face turning experiments on a precipitation hardened IN718 nickel-based alloy, in order to compare the experimental results with the forces and stresses predicted from 3-D finite element simulations. At the same cutting conditions and residual stress profiles were measured by using the X-ray diffraction technique and utilized in comparison of machining induced stress profiles obtained from 3-D FE simulations. They used the Deform-3D FE software with Johnson-Cook model which was modified to include flow softening. The authors concluded that these simulations provide closer results to the experimental results and also discussed the effects of various cutting parameters on the residual stresses.

2.4 Smoothed Particle Hydronamics (SPH): A New Technique for Modeling Machining

Heinstein and Segalman [25] at the Sandia National Laboratories, developed one of the first orthogonal metal cutting simulations based on the method of smoothed

particle hydrodynamics (SPH). The study provided a new alternative to the traditional finite element techniques that are conventionally used. The authors concluded that the SPH technique proves to be more promising in simulating the large deformations that happen near the tool, without the loss of stability and accuracy which is the case with finite element models.

Limido et al. [26] developed a high speed machining cutting model with the SPH method in `LS-DYNA` Code. The aim of this study was to demonstrate the merits of the SPH method such as natural chip/workpiece separation, and also compared the result with experimental results. The authors also concluded that the SPH model was able to predict shear and continuous localized chip during each step of its formation and also predicts cutting forces with grated accuracy. A suggestion was made regarding the need to develop a 3D SPH model simulating oblique cutting.

Villumsen and Fauerholdt [27] also used the `LS-DYNA` finite element code to develop an SPH model for metal cutting. Their study provided certain critical techniques by which an SPH model can be built with the `LS-DYNA` software. They carried out a sensitivity analysis to demonstrate the effects of no of particles, mass scaling and time scaling. Moreover, they also conducted an analysis on the friction between the workpiece and tool and their effects on the cutting forces. Finally, they compared the obtained results with experimental data and concluded that the predicted cutting forces were more realistic and the simulated chip formation is more realistic. Furthermore, they expressed an interest in developing an SPH milling model to predict the cutting forces during the milling process.

Espinosa et al. [28] developed an orthogonal cutting, oblique cutting and milling model based on the SPH method with `LS-DYNA` finite element code. A comparison was made with Arbitrary Lagrangian-Eulerian (ALE) finite element models. The authors also provided some important specificities of the SPH model implementation such as the introduction of artificial viscosity, use of renormalized SPH formulation and gave

an incite on the numerical instabilities like tensile instability and zero energy modes. The conclusions from this study were in tune with the previous studies on SPH.

Madaj and Píška [29] used the `ANSYS LS-DYNA` solver to simulate orthogonal cutting on A2024-T351 Aluminum Alloy and compared the results with experimental and FEM simulation results. They conducted studies which demonstrated the influence of Johnson-Cook parameters, SPH density and cutting speeds (200-800 m/min). They mentioned the use of the minimum strain to failure to be set for good correlation with the experimental results. They stressed on the need of further investigation the different material model parameters and other material models to prove the usability of the SPH method.

Storchak et al. [30] developed an SPH orthogonal cutting model for AISI 1045 steel. They showed that only two SPH solver parameters had a significant effect on the machining variables which were, the initial particle density and time-step increase coefficient.

Xi et al. [31] developed both 2D and 3D models to simulate machining on Ti6Al4V alloy. The aim was to investigate chip formation and cutting forces. They simulated two sets of parameters under four different initial workpiece temperatures also conducted experiments for the same. The influence of initial workpiece temperature on the cutting forces and chip formation was studied. The results found were in agreement with the experimentally obtained data.

CHAPTER 3: METHODS AVAILABLE FOR MODELING MACHINING

The most important reasons for the need to model machining is firstly, to conduct the operation in an efficient manner and obtain a desired quality of the finished component, and secondly, to develop suitable designs of machine tools by studying the loads during the process. The performance of a finished component is directly linked to the efficiency and effectiveness of the machining operation that has been carried out on it. The process of machining can be understood by the knowledge of cutting process and the movement of the machine-tool. Structural dynamics has been successfully used in understanding the movement of the machine-tool, but the cutting process is much more complex and so, many techniques have been and are being developed to model this phenomenon [32].

Apart from the experimental techniques, there have been various analytical methods to model the machining process. Early methods tried to explain the process in simple terms, by various assumptions, approximations and graphical representations [4–6]. Consecutive methods, consider the complex and nonlinear aspects of the cutting process such as thermal softening, shear bands, the secondary shear zone, etc [33]. As the considerations and calculations became complex, suitable techniques like finite element methods were employed. The various techniques to model the machining process have been briefly explained below.

3.1 Analytical Method

Even though many researchers are working to develop appropriate analytical methods to model the machining process, it is considered as a predecessor of numerical methods. They provide the basis for the concepts of finite element methods. Impor-

tant literature on the mechanics of the machining process include theories on the shear zone models, slip line theories, plasticity [3, 33]. Some of these theories are described below.

3.1.1 Shear Plane Model

According to this model the chip formation takes place by shearing taking place along a shear plane, which is inclined at an angle φ with the horizontal. It is also assumed that the chip remains in contact with the tool and is straight. The flow stress of the material is equal to the shear stress along the shear plane. The forces between the tool-chip interface are considered to be in equilibrium. This is shown in the Merchant's force diagram, see figure 2.6.

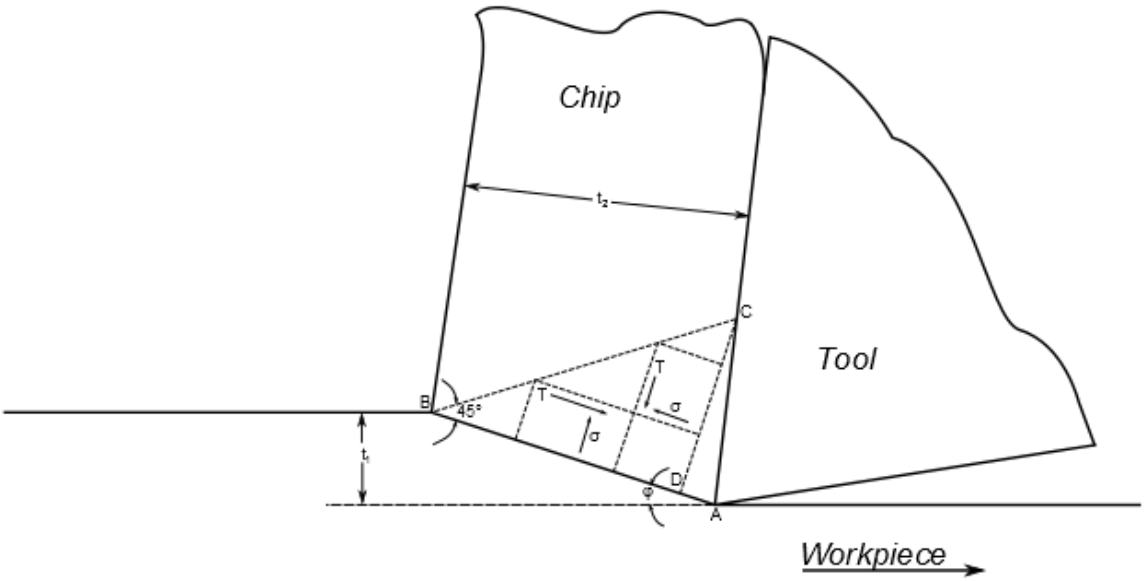

Figure 3.1: Slip line field model by Lee and Shaffer [35].

3.1.2 Slip-Line Field Models

In this approach the plastic deformation can be modeled in the plane strain without the consideration of elasticity (by quasi-static loading), by considering the workpiece as a rigid-plastic material. Elasticity is not included and the loading has to be quasi-static [34]. The slip-line is defined as a line that is curved and tangential to the

maximum shear stress of the material.It was first developed by Lee and Shaffer [35] The slip-line field is a set of slip-lines in the plastic region if the workpiece during deformation. This theory defines the relationship between the unyielded and yielded region of the material (See Figure 3.1). The generalized solution is given below [33]:

The shear angle is calculated as,

$$\varphi + \rho - \gamma = \frac{\pi}{4} \tag{3.1}$$

and therefore,

$$2\varphi_{sp} + \rho - \gamma \approx \frac{\pi}{2} - \psi_{sp} \tag{3.2}$$

where, φ_{sp} is the specific shear angle and ψ_{sp} is the angle of inclination of the tangent to the plastic zone outer boundary.

3.1.3 Shear Zone Model

This model considers that the deformation takes place along a shear band and strain hardening effects are taken into consideration. The friction along the chip-tool interface is not considered to be constant. The most noted work on this model was done by Oxley [36]. It was deduced that the shear zone width was approximately one-tenth that of the length. From the variations in velocity the strain rates can be derived and can be calculated along with the strain (by integrating the strain-rate with respect to time) at each point in the primary deformation zone. This methodology is a reused to find the strains and strain-rates in the secondary deformation zone. The shear zone model proves to be an upgrade over the earlier models.

3.2 Numerical Methods

The limitations of the analytical methods and the complexity of the physics of the machining process encouraged researchers to develop numerical methods as a modeling technique. Finite element methods have proved to be successful in improving the accuracy of the machining models. The various types of numerical techniques to build

machining models with FEA are described below.

3.3 Types of Formulations Numerical Models

The machining process which typically involves large deformations and high strain-rates are modeled with the finite element methods using three commonly used formulations i.e., the Lagrangian formulation, the Eulerian formulation and the Arbitrary Lagrangian-Eulerian (ALE) formulation, with the addition of a fourth technique i.e., the Smoothed Particle Hydrodynamics (SPH) formulation, that has been of recent interest.

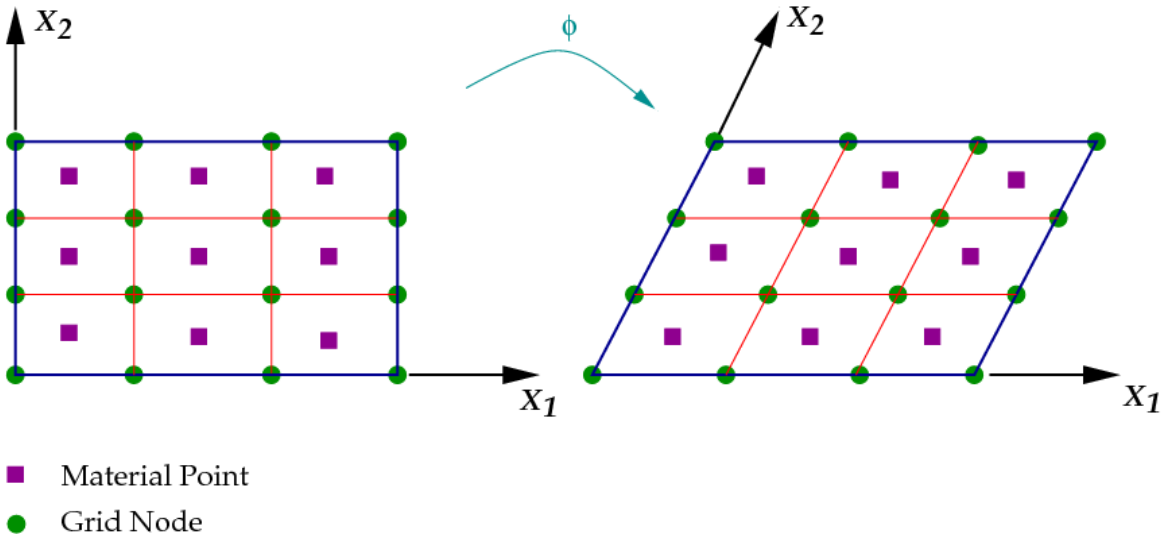

Figure 3.2: A Lagrangian mesh [37].

3.3.1 Lagrangian Formulation

In this formulation the finite element mesh is attached to the material. This is one of the earliest formulations used to model the machining process. During the machining process simulations, the mesh deforms with the material. As the mesh deforms, it undergoes high distortion thus, leading to numerical instability. To govern when the plastic deformation would take place, we define a chip formation criterion in the Lagrangian analysis. The advantages of the this method are that the computation time is faster and the chip geometry need not be predefined as it forms due to the

evolution of the physical deformation process [11, 38, 39]. A representation of the Lagrangian mesh has been shown in Figure 3.2.

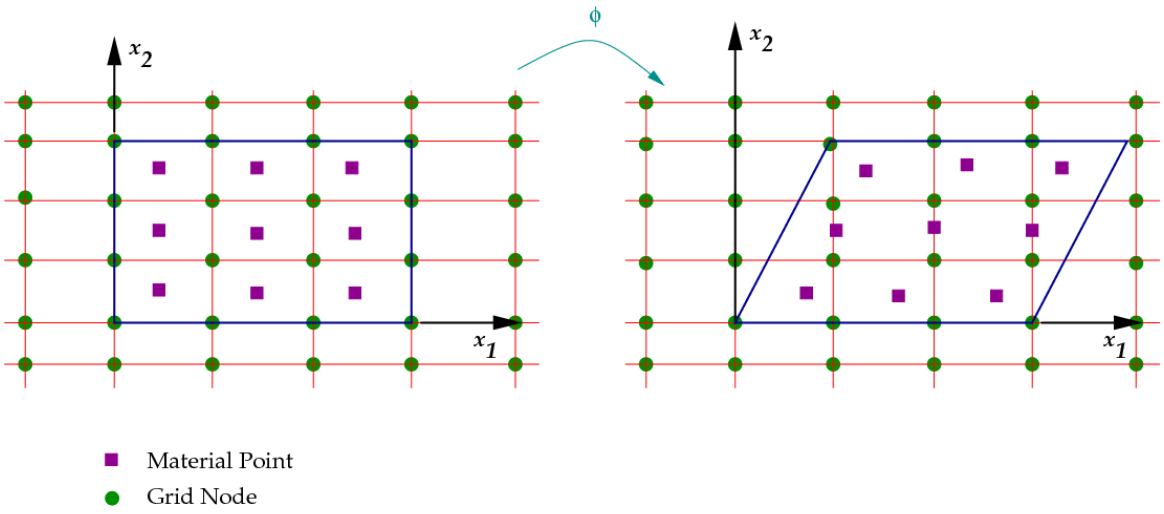

Figure 3.3: An Eulerian mesh [37].

3.3.2 Eulerian Formulation

In this formulation the mesh remains in place and the material moves through it during deformation. This is generally done in two steps in which the material deforms with a Lagrangian formulation and then the deformation is mapped on the constant Eulerian mesh. The merits of this formulation are that there are no errors due to mesh distortions that can affect the magnitude of strains predicted in the simulation. Also, there is no need to provide a separation/fracture criteria as the material properties governs the deformation. Fewer elements are required when this formulation is used. The above advantages lead to a lower computation time and the continuous flow of the material is also well predicted. The limitations of this formulation include the inability to simulate free surfaces and discontinuous chips as the mesh is fixed. Figure 3.3 shows an Eulerian mesh. The Eulerian formulation is not preferred to simulate solid mechanics problems such as the machining process, compared to the Lagrangian formulation [11, 38, 39].

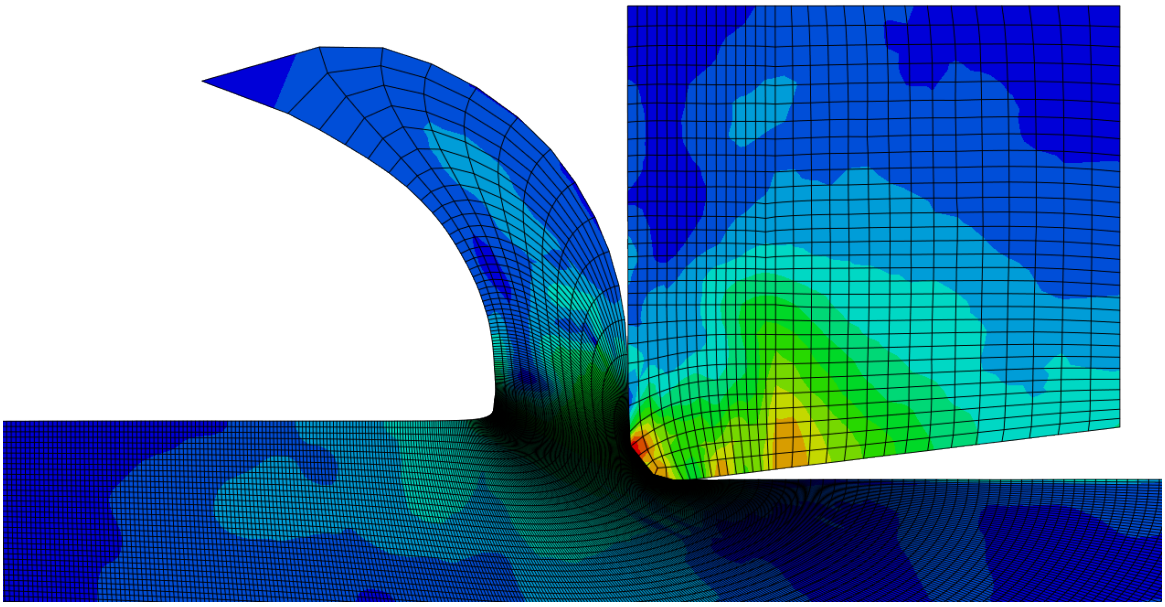

Figure 3.4: An Arbitrary Lagrangian-Eulerian (ALE) machining simulation [38].

3.3.3 Arbitrary Lagrangian-Eulerian (ALE) Formulation

The most preferred finite element formulation that is used to model large deformation problems like the machining process, utilizes the best of both the Lagrangian as well as the Eulerian formulations. It is known as the Arbitrary Lagrangian-Eulerian (ALE) formulation. Remeshing is used in this formulation to reduce the element distortion and obtain a smooth mesh, but this feature comes at the cost of higher computation time. This formulation proves to be more accurate in predicting contact, chip formation, strain, strain-rate, temperature and cutting forces. An example of the ALE mesh used model the machining process has been shown in Figure 3.4.

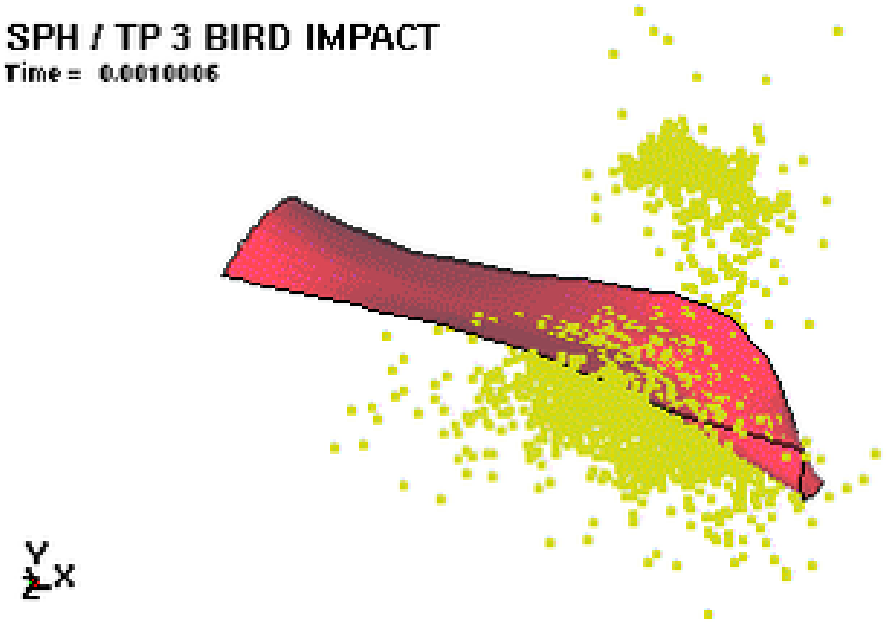

Figure 3.5: SPH simulation of a projectile impact on a turbine blade [40].

3.3.4 Smoothed Particle Hydrodynamics (SPH)

The SPH Method belongs to the class of numerical methods collectively known as meshless or mesh-free methods. These methods have become popular due to their ability to handle severe deformations while avoiding mass and energy losses encountered by traditional finite element methods. In the SPH method, the given domain is discretized into a set of particles and the material properties and the field variables are assigned to each of these particles. The method has been implemented in many commercial finite element packages such as `LS-Dyna` [1] and `ABAQUS` [2]. In the recent years, there has been an increased interest amongst many researchers to model the machining process by the SPH method due to its many merits. As this formulation is based on the Lagrangian system, it is capable of capturing the history of the material such as damage, without diffusion errors due to advection, that are seen with the Eulerian formulation.

Lucy [41], Gingold and Monaghan [42] developed the Smoothed Particle Hydrodynamics (SPH) method to simulate problems related to astrophysics. The most important merit of their work was that the SPH method did not require a mesh to

compute the derivatives. Subsequently, Monaghan [44], Benz [45] and Belytschko et al [43] reviewed the initial developments of the SPH method. Furthermore, The SPH method with solid mechanics was implemented in $2D$ and $3D$ by researchers like Libersky and Petschek [46,47], and were then merged with conventional finite element codes [48,49].

The basic SPH formulation contained many pitfalls such as tensile instability, lower accuracy, lower consistency, artificial viscosity and zero energy modes. In the recent past some, but not all shortcomings have been resolved by [50,51]. An application of the SPH formulation to simulate a projectile impact on a turbine blade is shown in Figure 3.5. The basics of the SPH formulation from [50] has been provided below.

3.4 The Smoothed Particle Hydrodynamics (SPH) Formulation

3.4.1 Basic Formulation

The Smoothed Particle Hydrodynamics (SPH) formulation uses a kernel interpolation function instead of a finite element mesh, to compute the state variables at any point in the system. An example of this, is the value of the continuous function $f(x)$ at any x, which is approximated by an integral of the product of a kernel (Weight) function and the function itself. It is given by $W(x—x', h)$ as,

$$\langle f(x)\rangle = \int W(x—x', h) f(x'). \tag{3.3}$$

Here, the kernel approximation is denoted by $\langle\rangle$, h is the smoothing length that defines the size of the kernel support and x' is the updated independent variable.

The kernel function is zero everywhere except a finite set of points included in the range of smoothing length $2h$ as,

$$W(x—x', h) = 0 \text{ for } \ |x—x'| >= 2h. \tag{3.4}$$

Once normalized we have,

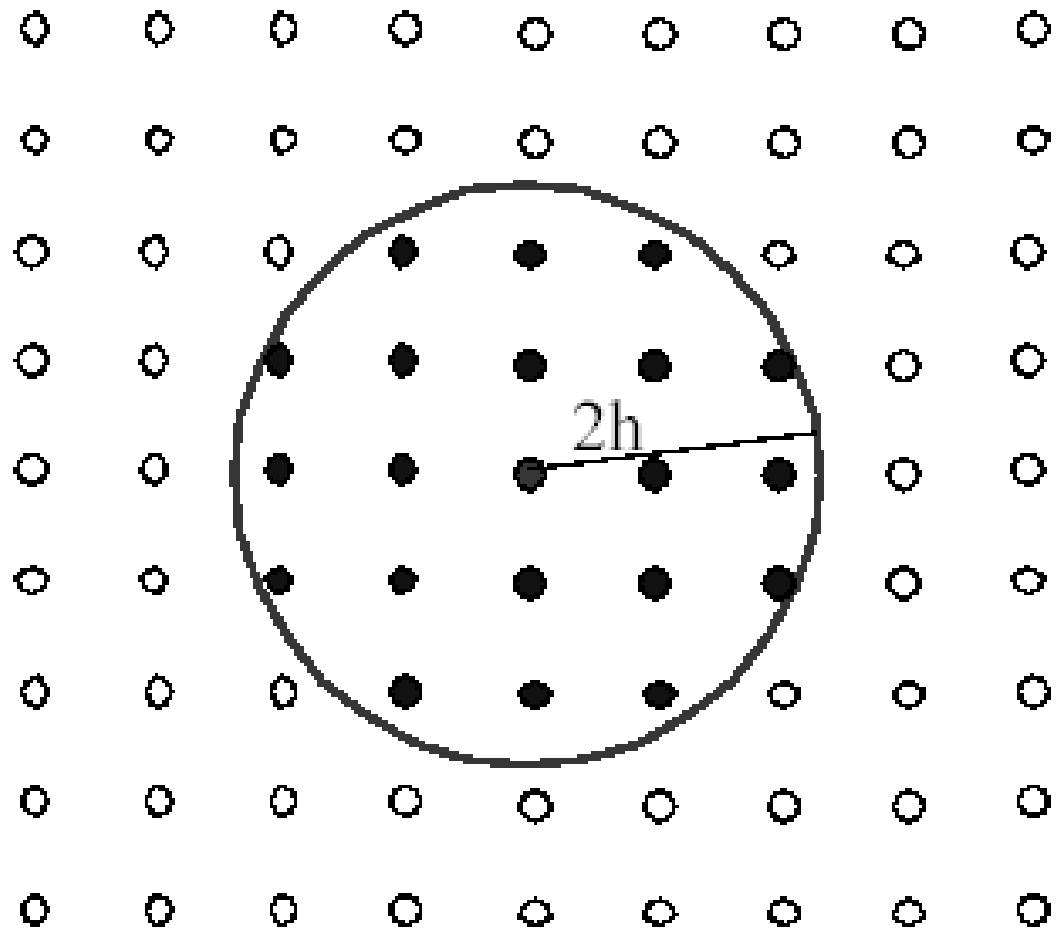

Figure 3.6: A set of neighboring particles [50].

$$\int W(x—x', h)dx' = 1. \tag{3.5}$$

The following formulations by Lucy [41], make sure that when h tends to zero, the kernel function converts into the Dirac delta function as,

$$\lim_{h\to 0} W(x—x', h) = \delta(x—x', h) \tag{3.6}$$

and so,

$$\lim_{h \to 0} \langle f(x) \rangle = f(x). \tag{3.7}$$

If f(x) is known only at N discrete points, the integral of equation 3.3 is approximated using a summation as,

$$\langle f(x) \rangle = \sum_{j=1}^{N} \frac{m^j}{\rho^j} f(x^j) W(x—x^j, h) \tag{3.8}$$

and so,

$$\langle f(x^i) \rangle = \sum_{j=1}^{N} \frac{m^j}{\rho^j} f(x^j) W(x^i—x^j, h) \tag{3.9}$$

where, $\frac{m^j}{\rho^j}$ is the volume of the particle j. Thus the basic SPH method is given by equation 3.8. We see from equation 3.9 that at any particle i, the value of a variable is computed by the contributions from the neighboring particles j where, the kernel function is non zero (see Figure 3.6).

3.4.2 Conservation Equations

Now, the conservation equations in the Lagrangian system are given as,

$$\frac{d\rho}{dt} = -\rho \frac{\partial V_\alpha}{\partial x_\alpha} \tag{3.10}$$

and

$$\frac{dV_\alpha}{dt} = \frac{1}{\rho} \frac{\partial \sigma_{\alpha\beta}}{\partial x_\beta} \tag{3.11}$$

or

$$\frac{dV_\alpha}{dt} = \frac{\partial}{\partial x_\beta} \left(\frac{\sigma_{\alpha\beta}}{\rho} \right) + \frac{\sigma_{\alpha\beta}}{\rho^2} \frac{\partial \rho}{\partial x_\beta} \tag{3.12}$$

and

$$\frac{dE}{dt} = \frac{\sigma_{\alpha\beta}}{\rho} \frac{\partial V_\alpha}{\partial x_\beta} \tag{3.13}$$

or

$$\frac{dE}{dt} = \frac{\sigma_{\alpha\beta}}{\rho^2}\frac{\partial(\rho V_\alpha)}{\partial x_\beta} - \frac{\sigma_{\alpha\beta}V_\alpha}{\rho^2}\frac{\partial \rho}{\partial x_\beta} \tag{3.14}$$

where, $V_\alpha = \frac{dX_\alpha}{dt}$ and the components are denoted by α and β. The equations 3.12 and 3.14 were proposed by [44]. The SPH form of the conservation equations can be derived by the kernel interpolation as,

$$\left\langle \frac{d\rho}{dt} \right\rangle = -\int W\rho' \frac{\partial V'_\alpha}{\partial x'_\alpha} dX', \tag{3.15}$$

$$\left\langle \frac{dV_\alpha}{dt} \right\rangle = \int W \frac{\partial}{\partial X'_\beta}\left(\frac{\sigma'_{\alpha\beta}}{\rho'}\right) dx' + \int W \frac{\sigma'_{\alpha\beta}}{\rho'^2}\frac{\partial \rho'}{\partial x'_\beta} dx', \tag{3.16}$$

and

$$\left\langle \frac{dE}{dt} \right\rangle = \int W \frac{\sigma'_{\alpha\beta}}{\rho'^2}\frac{\partial\left(\rho' V'_\alpha\right)}{\partial x'_\beta} dx' + \int W \frac{\sigma'_{\alpha\beta}V'_\alpha}{\rho'^2}\frac{\partial \rho'}{\partial x'_\beta} dx'. \tag{3.17}$$

These are of the form,

$$\int W f(x')\frac{\partial g(x')}{\partial x'} dx'. \tag{3.18}$$

From the Taylor series expansion about $x' = x$ we get,

$$\int W f(x')\frac{\partial g(x')}{\partial x'} dx' = \int \left[f(x)\frac{\partial g(x)}{\partial x} + (x - x')\frac{d}{dx}\left(f(x)\frac{\partial g(x)}{\partial x} \right) + ... \right] W dx'. \tag{3.19}$$

The parts with odd powers of $x - x'$ get canceled as w is an even function. We now neglect second and higher order terms, keeping the consistency with the order of the method as,

$$\int W f(x')\frac{\partial g(x')}{\partial x'} dx' = \left(f(x')\frac{\partial g(x')}{\partial x'} dx' \right)_{x'=x}. \tag{3.20}$$

We now substitute the approximation $\left\langle \frac{\partial g(x)}{\partial x} \right\rangle$ in place of $\frac{\partial g(x)}{\partial x}$ and get,

$$\left(f(x') \frac{\partial g(x')}{\partial x'} \right)_{x'=x} = f(x) \int W \frac{\partial g(x')}{\partial x'} dx'. \tag{3.21}$$

The last relations from equations 3.15, 3.16 and 3.17 are used to get,

$$\left\langle \frac{d\rho}{dt} \right\rangle = -\rho \int W \frac{\partial V'_\alpha}{\partial x'_\alpha} dx', \tag{3.22}$$

$$\left\langle \frac{dV_\alpha}{dt} \right\rangle = \int W \frac{\partial}{\partial x'_\beta} \left(\frac{\sigma'_{\alpha\beta}}{\rho'} \right) dx' + \frac{\sigma_{\alpha\beta}}{\rho^2} \int W \frac{\partial \rho'}{\partial x'_\beta} dx' \tag{3.23}$$

and

$$\left\langle \frac{dE}{dt} \right\rangle = \frac{\sigma_{\alpha\beta}}{\rho^2} \int W \frac{\partial \left(\rho' V'_\alpha \right)}{\partial x'_\beta} dx' - \frac{\sigma_{\alpha\beta} V_\alpha}{\rho^2} \int W \frac{\partial \rho'}{\partial x'_\beta} dx'. \tag{3.24}$$

The spatial derivatives of kernel approximation are,

$$\left\langle \frac{\partial f(x)}{\partial x_\alpha} \right\rangle = \int W \frac{\partial f(x')}{\partial x'_\alpha} dx'. \tag{3.25}$$

We now integrate by parts to get,

$$\left\langle \frac{\partial f(x)}{\partial x_\alpha} \right\rangle = W f(x) - \int f(x) \frac{\partial W}{\partial x'_\alpha} dx'. \tag{3.26}$$

We can rewrite the first term of the above equation as,

$$W f(x) = \int \frac{\partial \left(W f(x') \right)}{\partial x'} dx'. \tag{3.27}$$

By using the Green's theorem we get,

$$\int \frac{\partial \left(W f(x') \right)}{\partial x'} dx' = \int_S W f(x') n_i dS. \tag{3.28}$$

The above obtained surface integral is zero if the limits of integration are greater

than the compact support of W or if a zero value is assumed by the field variable at the free surface of the body. Modification to account for the boundary conditions are required if none of these criteria are satisfied.

It is to be noted that the derivatives of the kernel are substituted in place of the spatial derivatives of the field variables in equations 3.22, 3.23 and 3.24.

$$\int W \frac{\partial f(x')}{\partial x'_\alpha} dx' = -\int f(x) \frac{\partial W}{\partial x'_\alpha} dx' \tag{3.29}$$

therefore,

$$\left\langle \frac{d\rho}{dt} \right\rangle = \rho \int V'_\alpha \frac{\partial W}{\partial x'_\alpha} dx', \tag{3.30}$$

$$\left\langle \frac{dV_\alpha}{dt} \right\rangle = -\int \frac{\sigma'_{\alpha\beta}}{\rho'} \frac{\partial W}{\partial x'_\beta} dx' - \frac{\sigma_{\alpha\beta}}{\rho^2} \int \rho' \frac{\partial W}{\partial x'_\beta} dx' \tag{3.31}$$

and

$$\left\langle \frac{dE}{dt} \right\rangle = -\frac{\sigma_{\alpha\beta}}{\rho^2} \int \rho' V'_\alpha \frac{\partial W}{\partial x'_\beta} dx' + \frac{\sigma_{\alpha\beta} V_\alpha}{\rho^2} \int \rho' \frac{\partial W}{\partial x'_\beta} dx'. \tag{3.32}$$

The last step is to transform the continuous volume integrals to sum over discrete interpolated points. Thus, the most conventional form of the SPH discretized conservation equations are obtained after some rearrangements to improve consistency as,

$$\frac{d\rho}{dt} = \rho^i \sum_{j=1}^{N} \frac{m^j}{\rho^j} \left(V^j_\beta - V^i_\beta \right) \frac{\partial W^{ij}}{\partial x^i_\beta}, \tag{3.33}$$

$$\frac{dV^i_\alpha}{dt} = -\sum_{j=1}^{N} m^j \left(\frac{\sigma^j_{\alpha\beta}}{\rho^{2j}} - \frac{\sigma^i_{\alpha\beta}}{\rho^{2i}} \right) \frac{\partial W^{ij}}{\partial x^i_\beta} \tag{3.34}$$

and

$$\frac{dE^i}{dt} = -\frac{\sigma^i_{\alpha\beta}}{\rho^{2i}} \sum_{j=1}^{N} m^j \left(V^j_\alpha - V^i_\alpha \right) \frac{\partial W^{ij}}{\partial x^i_\beta}. \tag{3.35}$$

Here, $W^{ij} = W(x^i - x^j, h)$.

3.4.3 Choice of Kernel Function

Now we define the kernel function to finish the discretization. A large number of function types are available in the literature from polynomial to Gaussian, but the most conventional kernel used is the cubic B-spline proposed by Monaghan [44].

$$W(v,h) = \frac{C}{h^D} \times \begin{cases} \left(1 - \frac{3}{2}v^2 + \frac{3}{4}v^3\right) & v < 1, \\ \frac{1}{4}(2-v)^3 & 1 \leq v \leq 2, \\ 0 & \text{Otherwise.} \end{cases} \tag{3.36}$$

where, $v = \frac{|x-x'|}{h}$, D is the number of spatial dimensions, C is the scale factor that is responsible to confirm that the consistency conditions 2 and 3 are met, and depends on the D. Therefore, we have,

$$C = \begin{cases} \frac{2}{3} & D = 1, \\ \frac{10}{7\pi} & D = 2, \\ \frac{1}{\pi} & D = 3. \end{cases} \tag{3.37}$$

3.4.4 Variable Smoothing Length

Benz [45] suggested the use of a variable smoothing length in order to eliminate some of the demerits of constant smoothing length such as, less interaction of particles due to large deformation cause errors and higher interaction in compression and thus increase in computation time. Thus, the proposed change in h is given by,

$$h = h_o \left(\frac{\rho_o}{\rho} \right)^{\frac{1}{n}} \tag{3.38}$$

where, $\rho_\circ$ is the density, $h_\circ$ is the initial smoothing length and n is the number of spatial dimensions. Also, an alternative mass conservation dependent variable h equation is,

$$\frac{dh}{dt} = \frac{1}{n} h \, \mathrm{div}(v) \tag{3.39}$$

where, the divergence of velocity is denoted by $\mathrm{div}(v)$.

3.4.5 Neighbour Search

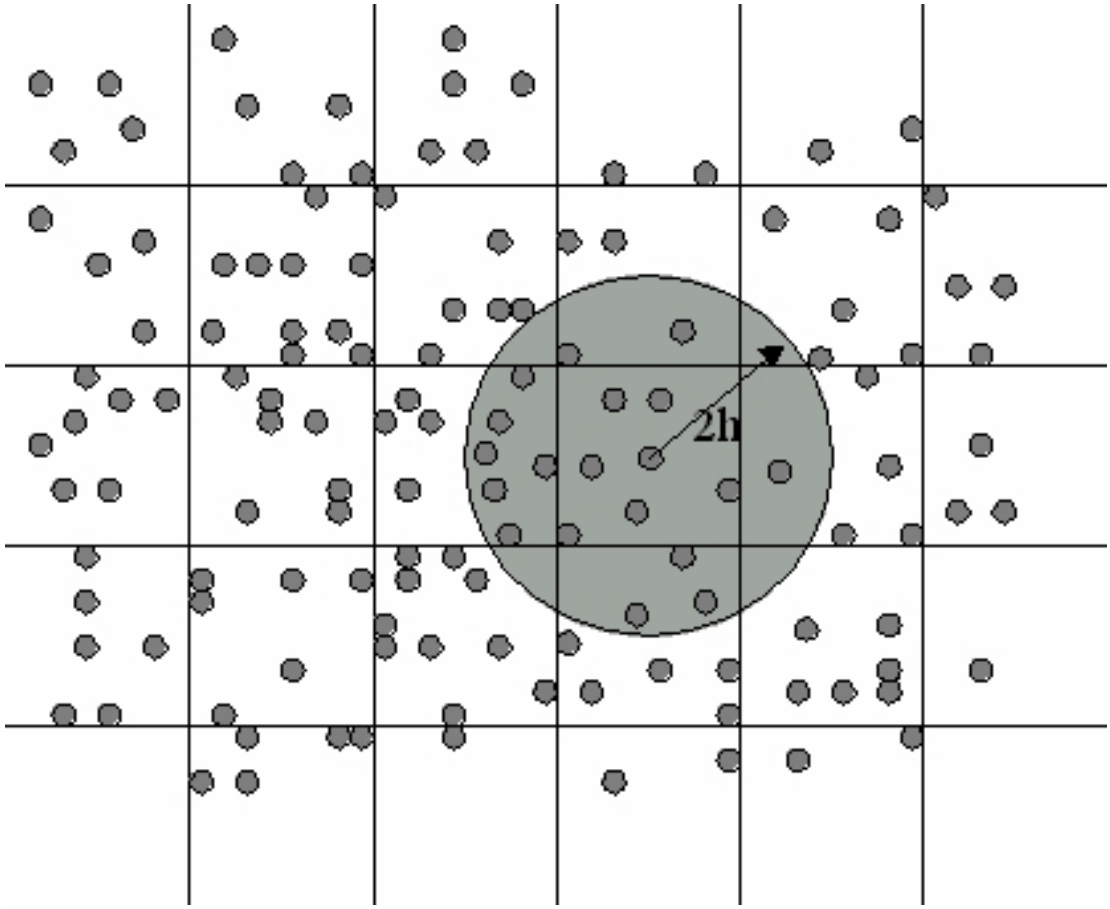

Figure 3.7: Neighbor search by the bucket sort method [50].

One of the important parts of the SPH simulation is the task of neighbor particle search. It is a time consuming and computationally heavy task and therefore, it has

to be performed in an efficient manner and so, a direct search method would prove to be futile. An efficient method is the bucket sort method. The particle are sorted according to a temporary mesh that is of size 2h (See Figure 3.7). Following this, for a particular particle, the neighbor particles in the same box and adjoining boxes are searched. This results in the results from the a reduction of computation time from N^2 (for direct search method) to $N \log N$ (in case of the bucket sort method), N being the total number of particles.

3.5 Pitfalls of the SPH Method

While modeling solid mechanics problems such as the machining process, the SPH formulation generally shows three problems namely,

1. Consistency
2. Tensile Instability
3. Zero-Energy Modes

3.5.1 Consistency

Deficiency of kernel support beyond length $2h$ of domain boundaries, results in the inconsistency of the continuous SPH method. If particles are irregularly distributed, then the method looses 0^{th} order accuracy over the whole domain. Therefore, the particles have to be defined as equally spaced as possible to maintain accuracy. Some of the corrective measures developed by various researchers to increase the order of consistency of the SPH method, have been discussed in [50].

3.5.2 Tensile Instability

Swegle et al [52] and Balsare [53] separately conducted a von Neumann stability analysis of the SPH method and found that it suffered from tensile instability. Tensile instability shows traits of fracture which is shown as a cluster of particles. This is actually a results from effective stress due to artificial negative modulus produced

from the correlation between the kernel interpolation and constitutive relation. The partial differential equations are changed due to this. From the stability analysis, it was found that the criteria for stability is $W''\sigma > 0$, where σ is the stress and W'' is the second derivative of W. This instability can also occur in compression, but is generally seen with tension as the minimum of the derivative is located at $2/3^{rd}$ the length of h, in the stability regime of the commonly used cubic B-spline kernel function. Some of the corrective measures suggested by various researchers to decrease the effect of tensile instability in the SPH method, have been discussed in [50].

3.5.3 Zero-Energy Modes

The Zero-Energy modes are similar to deformation modes featuring periodic nodal displacements producing zero strain energy. These types of features can be seen even with finite element and finite difference schemes. The cause of these modes is nodal under integration in which the derivatives of the field variables are calculated at the same point. The modes can be easily excited by quick, impulsive loading and are not resisted. Perhaps, the origins of these modes can be found in the fundamental SPH kernel function, which is an interpolation of a group of finite data on which sinusoidal waves can be fit, given the high enough magnitude of the order interpolation. Some of the corrective measures suggested by various researchers to decrease the effect of tensile instability in the SPH method, have been discussed in [50].

CHAPTER 4: SPH MACHINING MODEL WITH LS-DYNA

In the present work, the Smoothed Particle Hydrodynamics (SPH) technique has been used to model the orthogonal machining process on `AISI 1045` steel. The pre-processor `LS-PREPOST` of the commercial nonlinear finite element software `LS-DYNA` was used to build the SPH model as shown in the Figure 4.1.

Figure 4.1: SPH model of orthogonal machining of a `AISI 1045` steel workpiece with a carbide tool.

4.1 Geometry

The geometry (taken from [30]) of the workpiece was a rectangle of length 3.6 mm and width 0.3 mm. The workpiece was modeled with SPH particles defined by defining a rectangle of dimension 3.6 mm $\times$ 0.3 mm and providing a density of 7800 Kg/m^3 and particle spacing of 10 μm (see Figure 4.2). A total of 24300 SPH particles were produced. Each particle is provided with a mass based on the defined particle density. The particles are constrained in the Z direction to be consistent

Table 4.1: Material properties for Tungsten-carbide tool

Density Kg/m^3	15000
Young's Modulus (GPa)	800
Poisson's Ratio	0.2

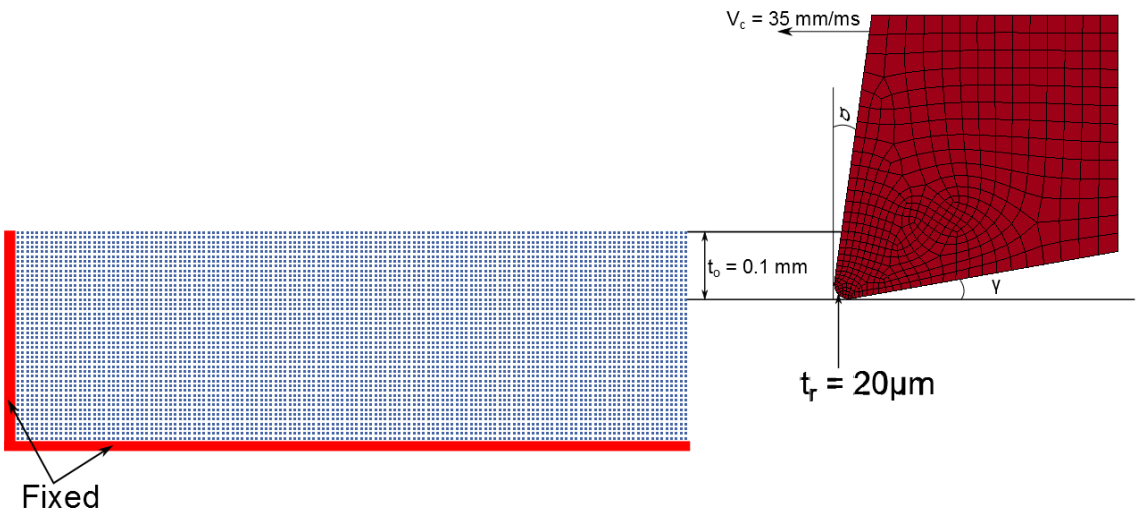

Figure 4.2: SPH model geometry.

with the assumptions in the orthogonal machining process which assumes plain strain conditions. Additionally, the nodes of on the bottom layer and the left side layer of the workpiece are constrained in the X and Y direction, which is a fixed boundary condition. The tool was modeled as a $3D$ rigid body of width 0.04 mm and with the material properties of tungsten-carbide, which are shown in Table 4.1. The tool was sketched using the design software `SolidWorks` and meshed in the finite element preprocessor `HyperMesh`. As the tool is modeled to be a rigid body, the mesh need not be fine. The tool was meshed with 8 node fully integrated S/R solid elements. The tool was constrained such that it can move only in the X direction. The tool was given a tool-tip radius of 20 μm and a rake and clearance angle of 8° and 10° respectively. The length of cut for the simulation was 3.5 mm and the total time for the simulation was 0.1 ms. A constant depth of cut of 0.1 mm was considered. The analysis with `LS-DYNA` was performed as an SPH-Solid structural only analysis because, SPH-Solid coupled structural-thermal analysis have not yet been found to provide reliable results. An artificially high cutting speed (20 times higher) of 35 m/sec was used [28] to reduce the numerical instabilities discussed in the previous chapter.

4.2 Constitutive Model & Material Properties

The `AISI 1045` steel workpiece was modeled with the Johnson-Cook plasticity model [54] and the various parameters were obtained from Jaspers [55]. In this model the flow stress is expressed as a function of yield stress, strain hardening, strain rate and temperature. The Johnson-Cook plasticity model is given by equation 4.1.

$$\sigma_{flow} = \left(A + B\varepsilon_{pl}^{n}\right)\left[1 + C\log\left(\frac{\dot{\varepsilon}_{pl}}{\dot{\varepsilon}_{o}}\right)\right]\left[1 - \left(\frac{\theta - \theta_{o}}{\theta_{melt} - \theta_{o}}\right)^{m}\right] \tag{4.1}$$

where, σ_{flow} is the flow stress, A is the material yield stress, B is the strength

Table 4.2: Material properties for `AISI 1045` Steel

A (MPa)	553
B (MPa)	600.8
n	0.234
C	0.013
m	1
Room temperature, θ_o°C	27
Melting temperature, θ_{melt}°C	1460
Reference strain rate, $\dot{\varepsilon_o}$ s^{-1}	1
Density Kg/m^3	7800
Shear modulus (GPa)	76.923
Bulk modulus (GPa)	166.67
Young's modulus (GPa)	200
Poisson's ratio	0.3
Specific heat (J/KgK)	432.6

coefficient, ε_{pl} is the effective plastic strain, n is the strain-hardening exponent, C is the strain rate constant, θ is the current temperature, θ_o is the room temperature, θ_{melt} is the melting temperature and m is the thermal softening exponent. Large deformations occurring during the orthogonal machining process are easily handled by the SPH formulation. The fracture/separation of the chip from the workpiece is handled by the SPH formulation in a more natural way than conventional Lagrangian finite element models. Therefore, no additional fracture/separation criterion needs to be defined. The above Johnson-Cook plasticity model parameters can directly be input to `LS-DYNA` with the `*MAT_JOHNSON_COOK` material card in a tabular form. The material parameters used in this study have been specified in Table 4.2.

4.3 Contact

The contact between the tool and workpiece was defined by the AUTOMATIC-NODES-TO-SURFACE card with the tool being the master and workpiece being the slave. The penalty type contact algorithm is used which monitors and avoids the intrusion of slave nodes into the master surface. During contact the coefficient of friction μ is given by,

$$\mu = \mu_D + (\mu_S - \mu_D)e^{-DC|v_{rel}|} \tag{4.2}$$

where, μ_S and μ_D are the coefficients of static and dynamic friction respectively, DC is the exponential decay coefficient, which governs the transition between the static and dynamic friction conditions, and v_{rel} is the relative velocity between the tool (master) and the workpiece (slave). In this model $\mu_S = 0.5$ and $\mu_D = 0.3$ and $DC = 0.1$. The bucket sorts and constraints were further defined in the *CONTROL_CONTACT card.

4.4 SPH Control Parameters

There are several parameters which are used to control an SPH simulation, some generic to the formulation and some related to the finite element package used. In

the present work, LS-DYNA is used to simulate the orthogonal machining process with the SPH method. *CONTROL_BULK_VISCOSITY, *CONTROL_SPH and *SECTION_SPH cards with the scale factor for computed time-step can be specified to control the simulation. In the conventional finite element method, the bulk viscosity is introduced to maintain stability of the solution when shocks or oscillations occur. For the conservation of momentum the SPH method also relies on the use of artificial viscosity. In LS-DYNA the bulk viscosity is defined by the *CONTROL_BULK_VISCOSITY card with two parameters, Q1 and Q2 [1]. By default the values of Q1 and Q2 are 1.5 and 0.06 respectively, but from various literature, it has been found that a value of 1.5 for Q1 and 0.5—1 for Q2 is used for SPH simulations [28, 56]. The type of SPH formulation, initial number of neighboring particles and the number of time-steps after which the particles are to be sorted can be defined in the *CONTROL_SPH card. A variable smoothing length is used by LS-DYNA to eliminate errors due to tension instability and also to reduce computation time [1, 50], with the initial smoothing length being h_o, which is taken as the maximum of the minimum distance between all the particles in the domain. The variable smoothing length is controlled by constants which are defined in the *SECTION_SPH card.

4.5 Equation of State

The equation of state term is used to define the hydrodynamic pressure-volume relations of the SPH domain. In the present work, the linear polynomial type of equation of state has been used. The pressure is given by,

$$P = C_o + C_1\mu + C_2\mu^2 + C_3\mu^3 + (C_4 + C_5\mu + C_6\mu^2)E \tag{4.3}$$

where, E is the internal energy, $\mu = \frac{\rho}{\rho_o} - 1$, and $\frac{\rho}{\rho_o}$ is the ratio between current density and reference density. Terms $C_2\mu^2$ and $C_6\mu^2$ are zero if $\mu < 0$ [1]. Here, only the C_1 term is used and all other terms are set to zero. The C_1 term is equal to the bulk

modulus of the workpiece material, i.e., of `AISI 1045` steel which is given in Table 4.2.

CHAPTER 5: RESULTS & DISCUSSION

In this chapter, the results obtained from the above described SPH orthogonal cutting model are presented with a discussion. Furthermore, the results from the various parametric studies are presented along with a discussion. The post processing of the various results was handled with `LS-PREPOST`.

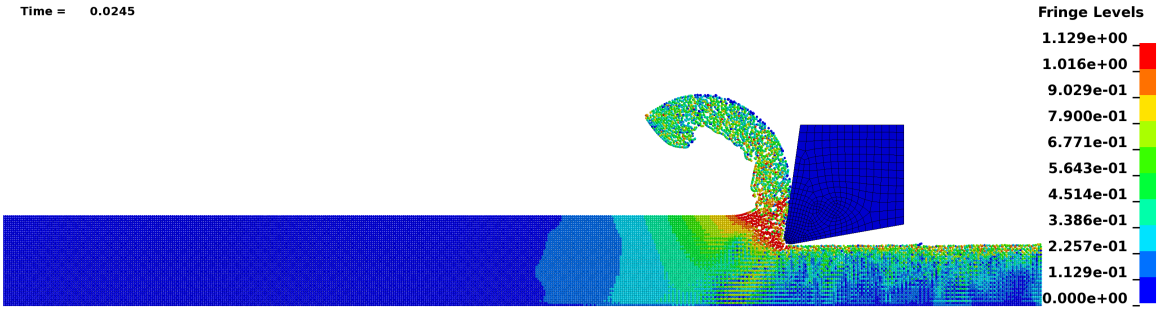

At time $t = 0.0245$ ms.

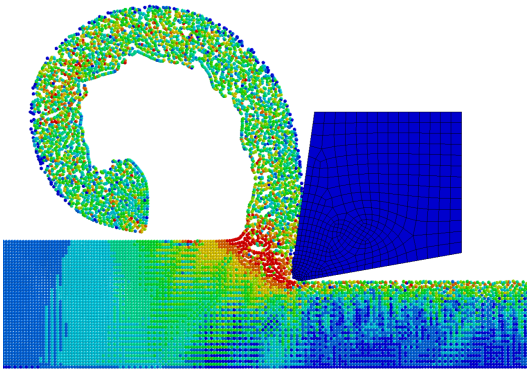

At time $t = 0.0495$ ms.

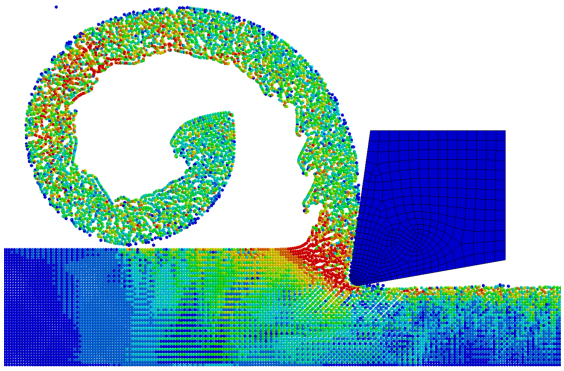

At time $t = 0.0745$ ms.

Figure 5.1: Distribution of von Mises stress (GPa) at various times during the machining operation showing the progression of chip formation.

5.1 SPH Model for Orthogonal Machining of AISI 1045 Steel

A continuous and naturally flowing chip morphology is observed as seen from Figure 5.1. The results from the SPH orthogonal machining model are discussed below.

5.1.1 Von Mises Stress

The contour plots of von Mises stresses at various times during the SPH orthogonal machining simulation are shown in Figure 5.1. Three cases are shown at time $t = 0.0245, 0.0495$ & 0.0745 sec. A maximum stress of 1.129 GPa is observed in the primary shear band region. The results obtained show good agreement with results previously obtained from numerical FEA simulation [57, 58] results.

5.1.2 Effective Plastic Strain

The contour plots for effective plastic strain at various times during the SPH orthogonal machining simulation are shown in Figure 5.2. Three cases are shown at time $t = 0.0245, 0.0495$ & 0.0745 sec. It is observed that the effective plastic strain predominantly shows values from 0.8 to 2, which causes workpiece material hardening. Plastic strain is observed to occur in both the primary as well as secondary shear zone.

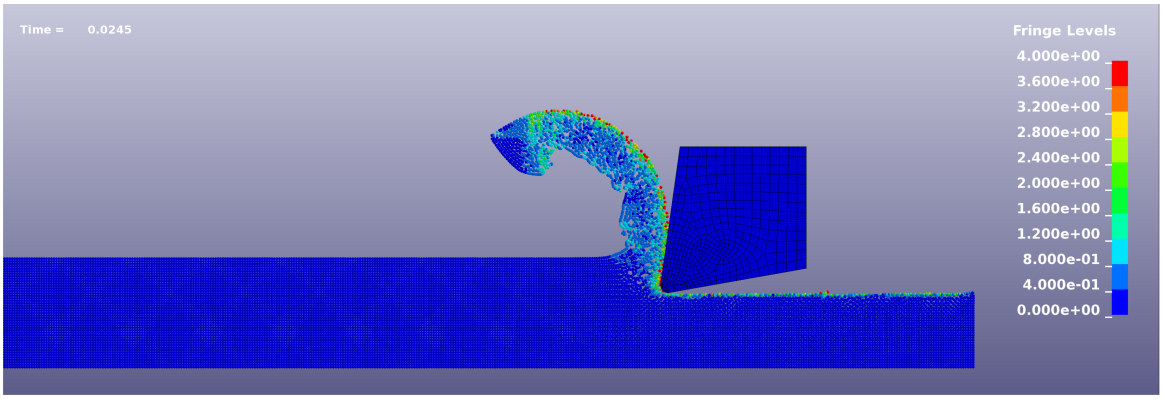

At time $t = 0.0245$ ms.

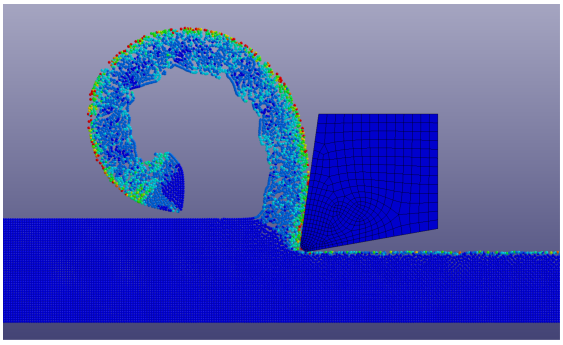

At time $t = 0.0495$ ms.

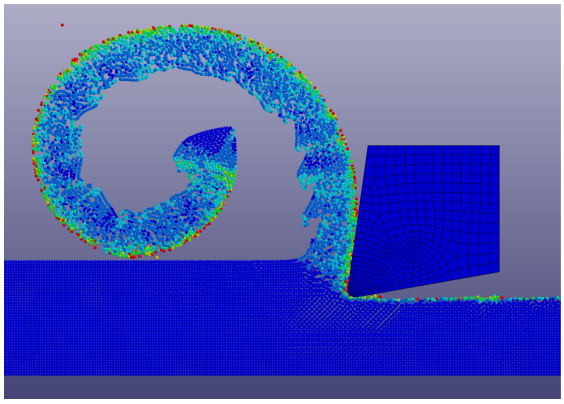

At time $t = 0.0745$ ms.

Figure 5.2: Contour plot of effective plastic strain at various times during the machining operation showing the progression of chip formation.

5.1.3 Cutting Force & Energy Balance

The cutting forces predicted by the SPH orthogonal machining model for `AISI 1045` steel are shown in Figure 5.3. The results obtained show good agreement with the results obtained by experimental and numerical FEA simulations [57, 58, 62]. The cutting forces during the machining process are observed to have an average value of 140 N.

To validate the results obtained by the SPH orthogonal machining model, it is important to have a balance between the total energy and external work. The energy balance plot obtained from the simulation is shown in Figure 5.4. The external work is observed to be approximately equivalent to the total energy of the system. The sum

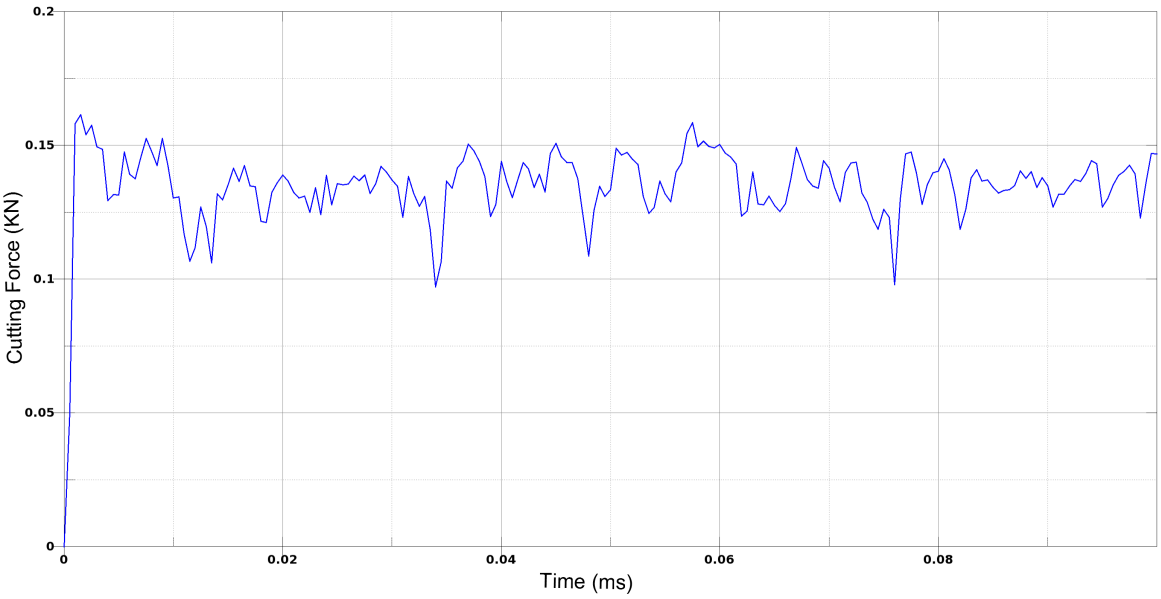

Figure 5.3: Predicted cutting force during the simulation of the orthogonal machining process on `AISI 1045` steel using the SPH method.

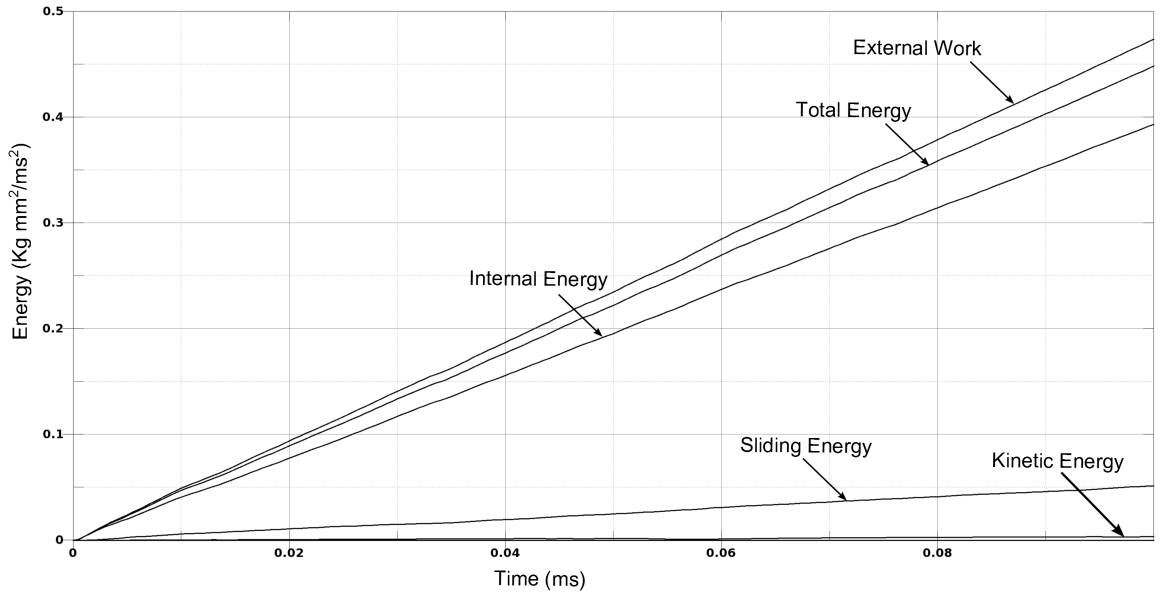

Figure 5.4: Energy balance during the simulation of the orthogonal machining process on `AISI 1045` steel using the SPH method.

of the kinetic energy of the moving tool and chip, and the internal energy contained in the deformed workpiece make up the total energy. From Figure 5.4, it is observed that the results obtained are valid.

5.2 Influence of SPH Control Parameters

To establish the accuracy and reliability of smoothed particle hydrodynamics simulation of orthogonal machining, various parametric studies are conducted.

5.2.1 Convergence Study

The convergence study is conducted by increasing the number of SPH particles and observing the change in the maximum von Mises stress achieved and comparing the obtained results with experimental data [62]. All features of the model, including the geometry, cutting conditions were kept the same and only the particle density was increased. As seen from Figure 5.5, it is observed that the computation time increased with the particle density while achieving solution convergence. Table 5.1 shows the different cases that were used to perform the convergence study.

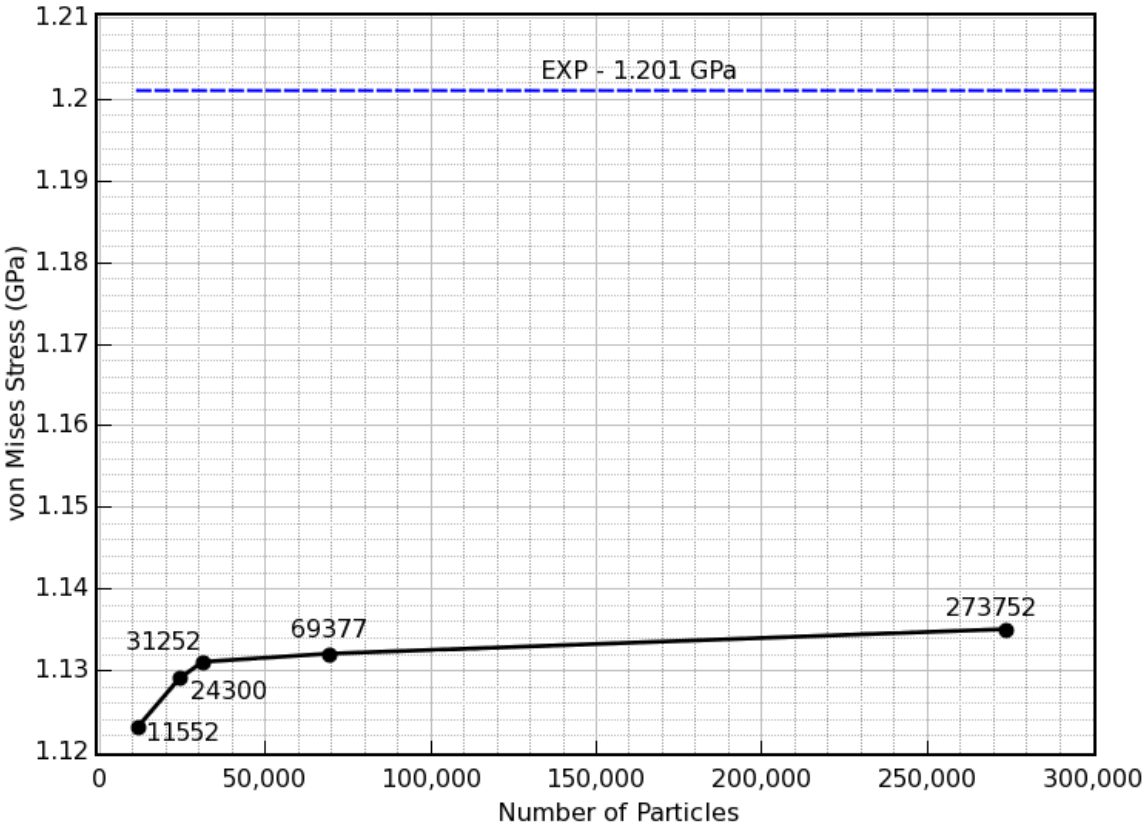

Figure 5.5: Convergence study by increasing the number of particles.

Table 5.1: Cases for convergence study.

Minimum distance between particles	Number of particles
10 μm	11252
6.667 μm	24300
5.88 μm	31252
4 μm	69377
2 μm	273752

5.2.2 Type of SPH Formulation

Recent literature shows that the default type of SPH formulation is inadequate and inconsistent, leading to unstable results and thus, modified SPH formulations such as the renormalization formulation show improved conservation [63]. Three such types of SPH formulations i.e., renormalization, default and total Lagrangian formulations are investigated.

From Figure 5.6, we see that only the renormalization SPH formulation gives a physical result and the default and total Lagrangian SPH formulations are inadequate to model orthogonal machining.

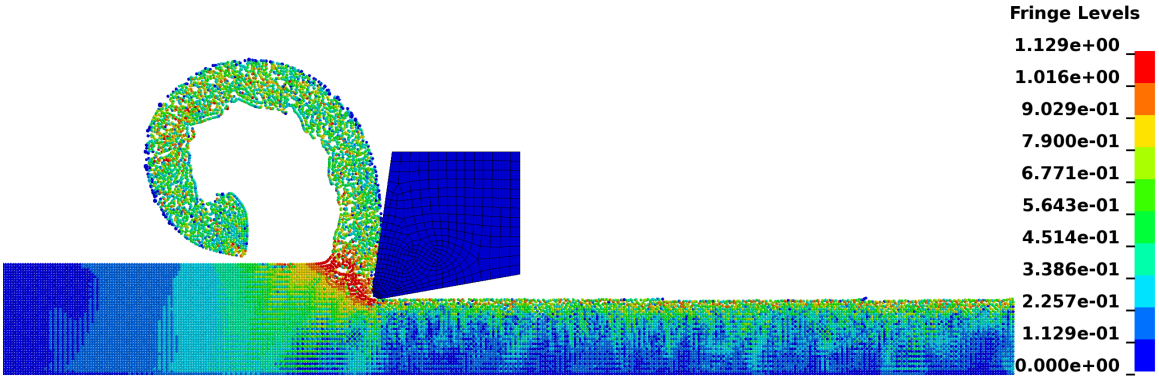

SPH renormalization formulation [1].

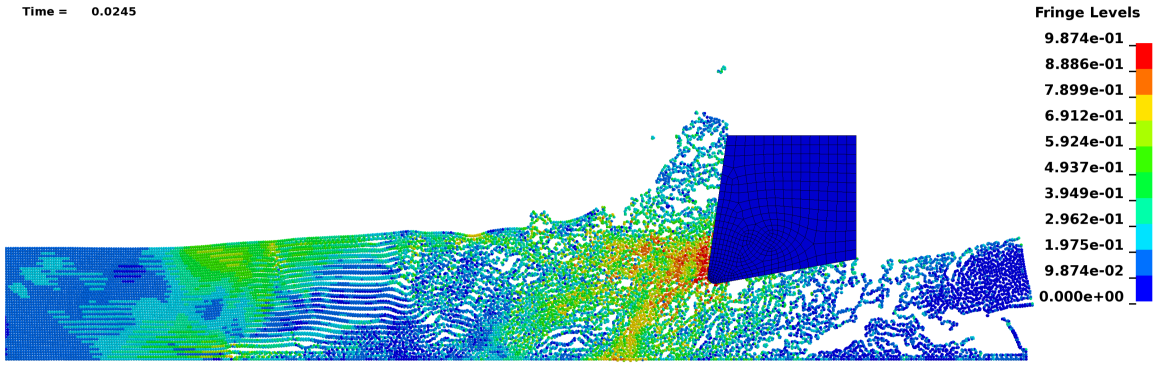

Default SPH formulation [1].

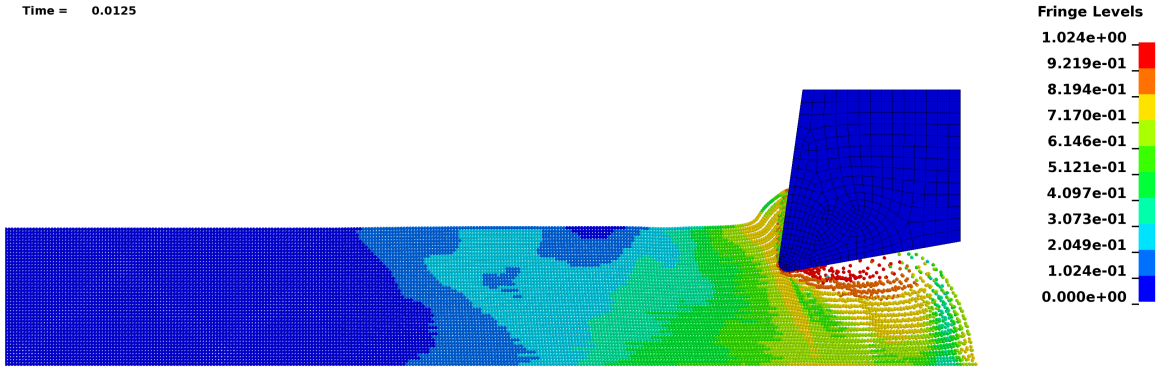

Total Lagrangian SPH formulation [1].

Figure 5.6: Contour plot of von Mises stress (GPa) for various types of SPH formulations available in `LS-DYNA`.

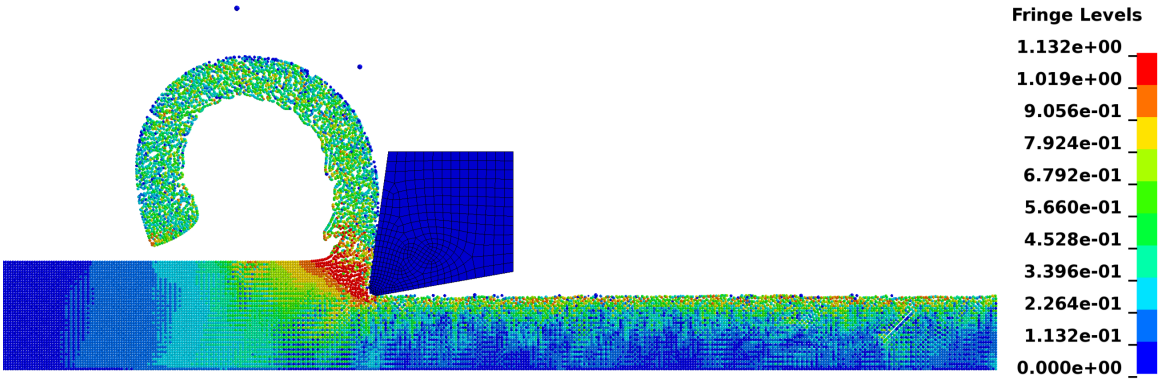

Scale factor for computed time-step 0.1.

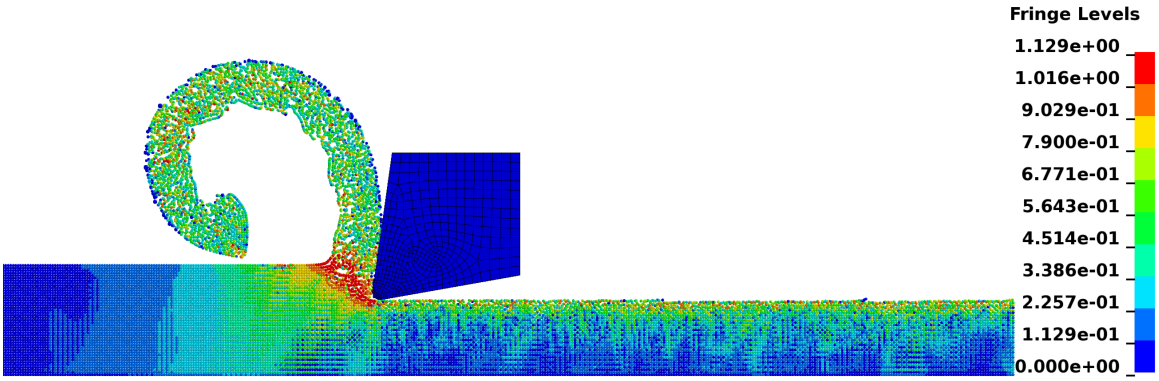

Scale factor for computed time-step 0.2.

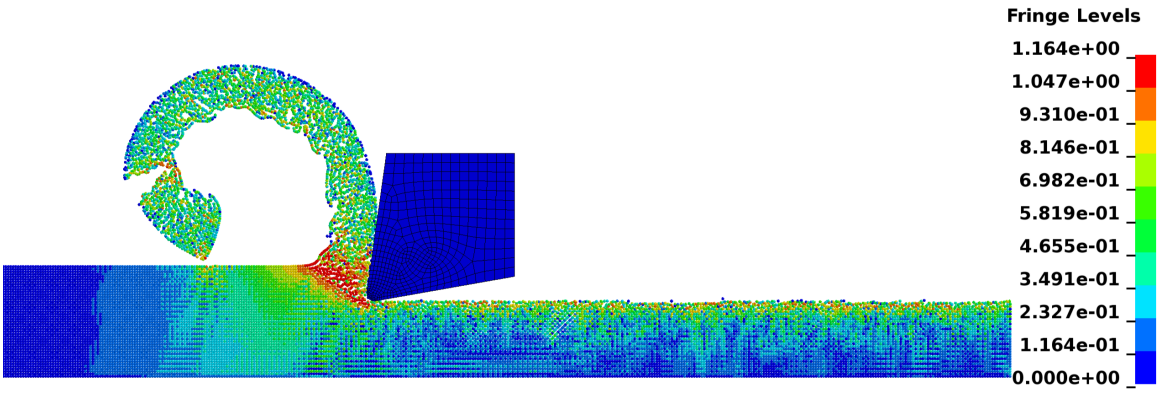

Scale factor for computed time-step 0.4.

Figure 5.7: Contour plot of von Mises stress (GPa) for various values of the scale factor for computed time-step.

5.2.3 Variation of Scale Factor for Computed Time-Step

One of the most important parameters that has an effect on the SPH orthogonal machining model is the scale factor for computed time-step. Effects are seen on the chip morphology as well as the computation time [30]. It is observed that the computation time decreases with increasing value of the scale factor for computed time-step. There also are changes observed in the chip morphology with respect to the chip curl radius and breaking of the chip. Figure 5.7 shows the cases with three different values of the scale factor for computed time-step.

5.2.4 Variation of Smoothing Length

Machining is a process during which large deformations occur and thus, while modeling the orthogonal machining process with the SPH method, the particles can move away from each other or new boundaries can form causing less interaction, and on the other hand, there is material being compressed just in front of the tool tip and rake face and this increases the computation time of the simulation. To fulfill the desire of having a uniform number of neighborhood particles, Benz [45] suggested the use of a variable smoothing length. `LS-DYNA` uses a variable smoothing length [1]. The effect of the variation of parameters in the *SECTION_SPH card, i.e., constants H_{min} and H_{max} and constant initial smoothing length (SPHINI) on the results were investigated. The various cases have been shown in Figure 5.8.

In the first case, it was observed that when the variability of the smoothing length was reduced by increasing the value of H_{min} and decreasing the value of H_{max}, the chip curl radius increased as the chip did not curl to contact the workpiece at $t = 0.0495$ mm, contrary to the case shown in Figure 5.1.

In the second case, the value of the initial smoothing length (SPHINI) is specified. Every particle is given a unique value of the initial smoothing length, which is determined by the software unless the SPHINI parameter is specified, and is taken to be the maximum of the minimum distance between every particle [1]. In this case the

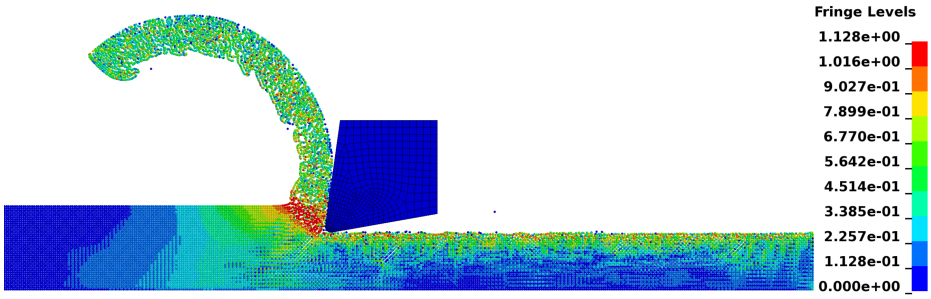

Case 1: The values of H_{min} and H_{max} have been increased and decreased respectively to reduce the variability of the smoothing length.

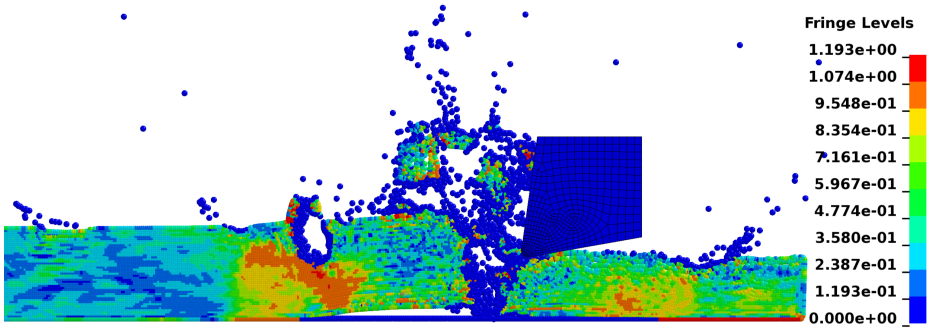

Case 2: A constant smoothing length of $0.02mm$ is used.

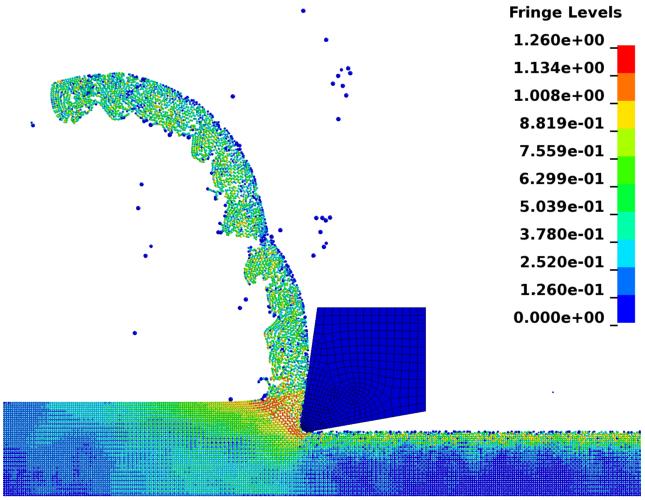

Case 3: A constant smoothing length of $0.005mm$ is used.

Figure 5.8: Contour plot of von Mises stress (GPa) for various smoothing length parameters.

value of parameter SPHINI was specified to be 0.02 mm, which is more than double the value in the base case. Due to non physical interactions between constitutive relations and kernel interpolations, tensile instability occurs which causes particles to

cluster and become unstable to a point which can lead to solution blowup [64]. An observation fitting to the above description is seen in this case.

In the third case, again the value of initial smoothing length (SPHINI) is specified to be 0.05 mm, which is about half of the value in the base case. Due to such a low smoothing length, there are less number of particle neighbors. This causes particles to fly out of the domain. This result is observed to be non-physical.

5.2.5 Use of Artificial Bulk Viscosity

For this study, the bulk viscosity coefficients, Q_1 and Q_2 were changed from the defaults and the results were compared with the case with default values. It is observed from Figure 5.9, that the contour plot for von Mises stress is more smooth in the case where the value of the coefficient Q_2 was changed to 0.5 which is in agreement with the findings by Espinosa et al. [28].

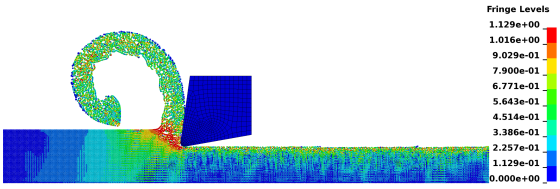

Default bulk viscosity coefficients i.e., $Q_1 = 1.5$ and $Q_2 = 0.06$.

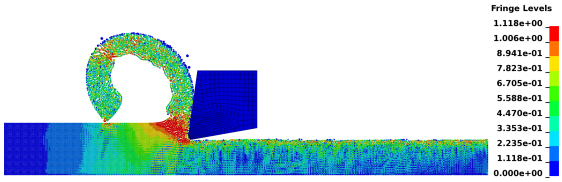

Bulk viscosity coefficients changed i.e., $Q_1 = 1.5$ and $Q_2 = 0.5$ [28].

Figure 5.9: Contour plot of von Mises stress (GPa) showing a comparison between the default and changed bulk viscosity coefficients.

5.3 Variation of Johnson-Cook Material Parameters

To investigate the effect of the constitutive model on the results, a parametric study with different Johnson-Cook material model parameters were used from the literature. All other parameters were kept the same. These material model parameters were obtained by various researchers using empirical data from the Hopkinson bar tests by considering large strain rates and adiabatic temperature rise due to plastic heating which cause material softening. The parameters by various authors is given in Table 5.2.

Table 5.2: Johnson-Cook parameters by various authors.

Author		A (MPa)	B (MPa)	n	C	m
Jaspers	[55]	553	600.8	0.234	0.013	1
Storchak	[30]	910	586	0.26	0.014	1.03
Özel	[59]	451.6	819.5	0.173	0.9×10^{-6}	1.095
Borkovec	[60]	375	552	0.457	0.020	1.4
Forejt	[61]	375	580	0.5	0.020	1.04

It is observed that due to the change in parameter A which is the yield stress of the material, the maximum stresses change in the contour plots. The chip morphology also changes with respect to chip curl radius, chip thickness and primary shear band thickness, due to the different values of B, n, C and m. The maximum stress obtained by using the parameters by Storchak, agrees with the results obtained in [30]. The results showing the different cases at three different times are shown in Figures 5.10, 5.11 and 5.12.

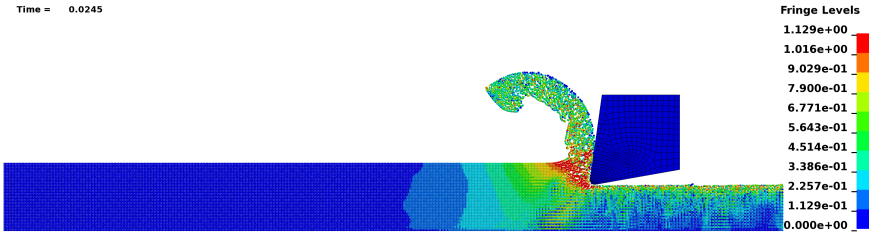

Jaspers [55].

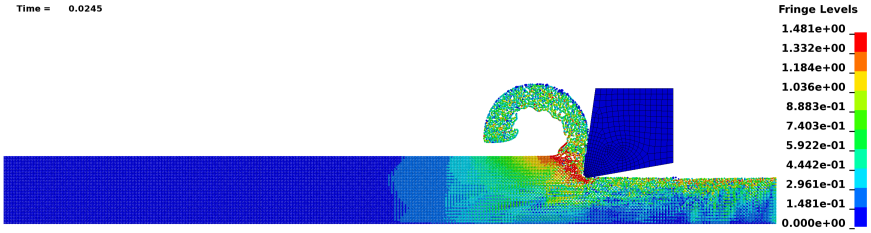

Storchak [30].

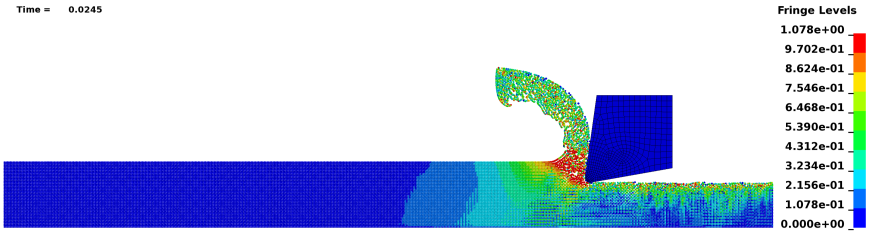

Özel [59].

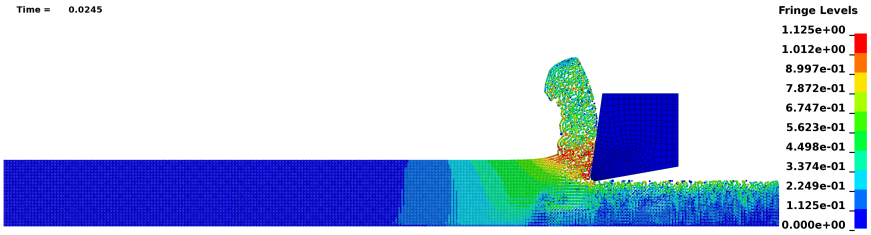

Borkovec [60].

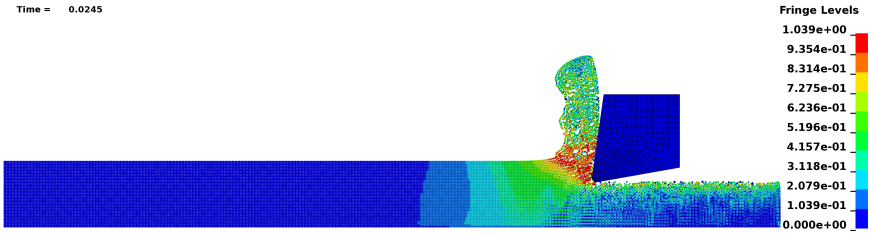

Forejt [61].

Figure 5.10: Contour plot of von Mises stress (GPa) using Johnson-Cook material parameters for `AISI 1045` steel from various authors at time $t = 0.0245$ ms.

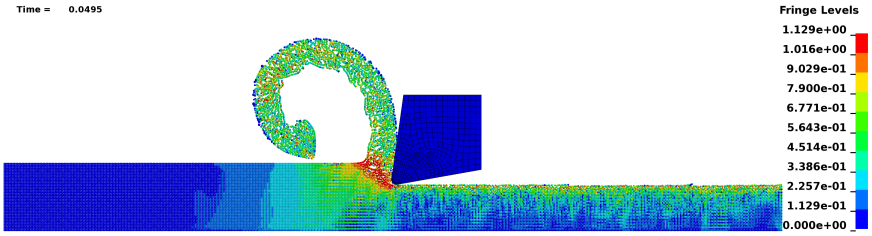

Jaspers [55].

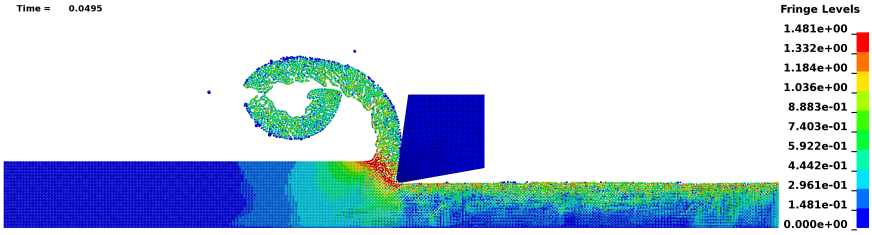

Storchak [30].

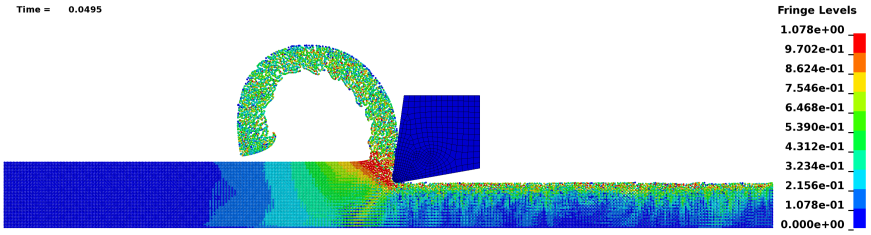

Özel [59].

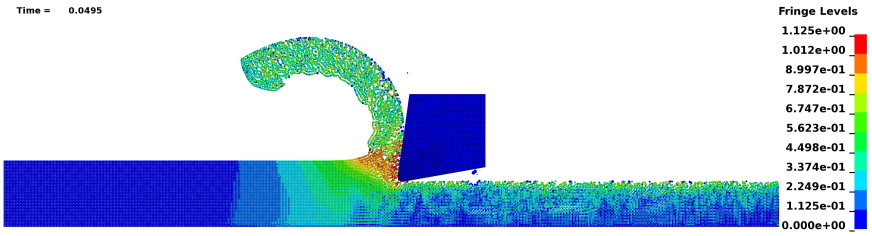

Borkovec [60].

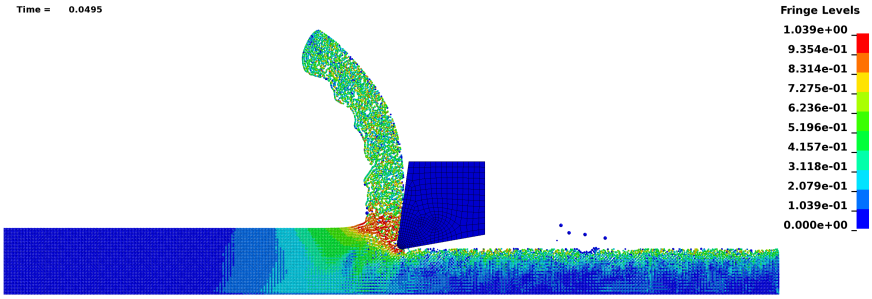

Forejt [61].

Figure 5.11: Contour plot of von Mises stress (GPa) using Johnson-Cook material parameters for `AISI 1045` steel from various authors at time $t = 0.0495$ ms.

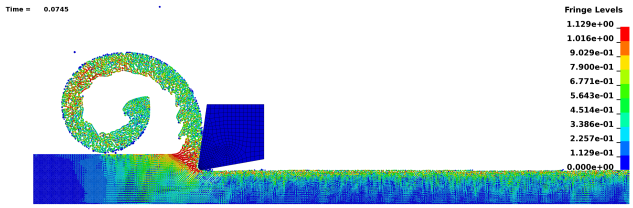

Jaspers [55]

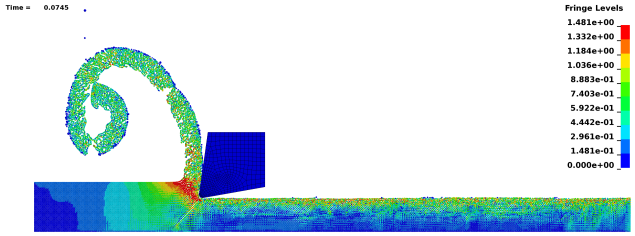

Storchak [30].

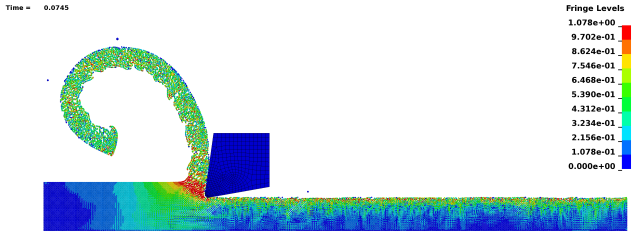

Özel [59].

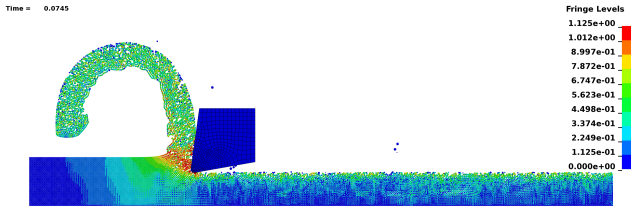

Borkovec [60].

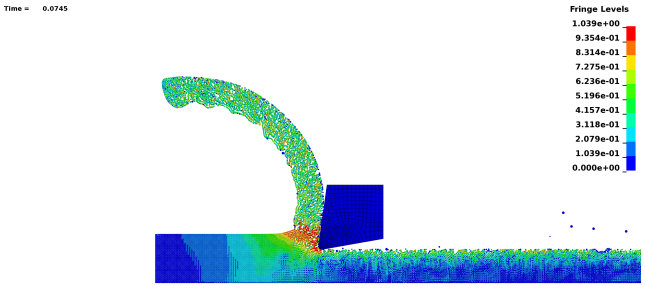

Forejt [61].

Figure 5.12: Contour plot of von Mises stress (GPa) using Johnson-Cook material parameters for `AISI 1045` steel from various authors at time $t = 0.0745$ ms.

5.4 Variation of Depth of Cut

To investigate the effect of the depth of cut on the results, a parametric study with different values of depth of cut was conducted. All other parameters were kept the same. The results show no significant change except for chip morphology. The various depth of cut cases at three different times are shown in Figures 5.13, 5.14 and 5.15.

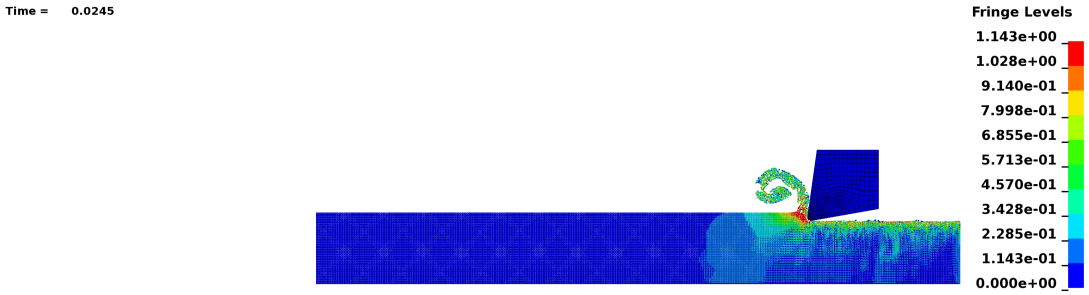

Depth of cut = 0.05 mm.

Depth of cut = 0.1 mm.

Depth of cut = 0.15 mm.

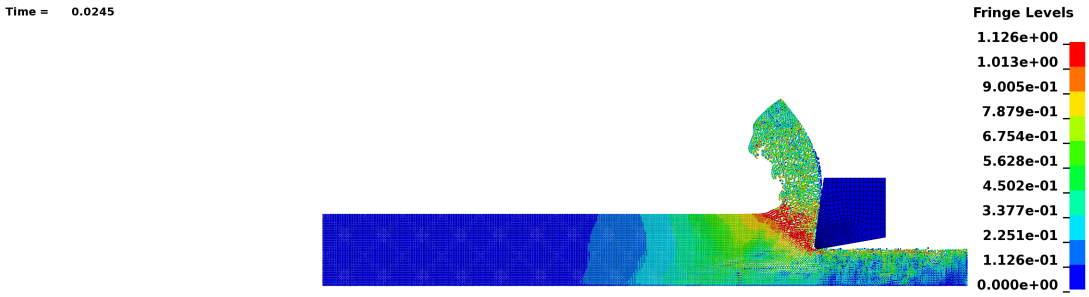

Depth of cut = 0.2 mm.

Figure 5.13: Contour plot of von Mises stress (GPa) for various depths of cut at time $t = 0.0245$ ms.

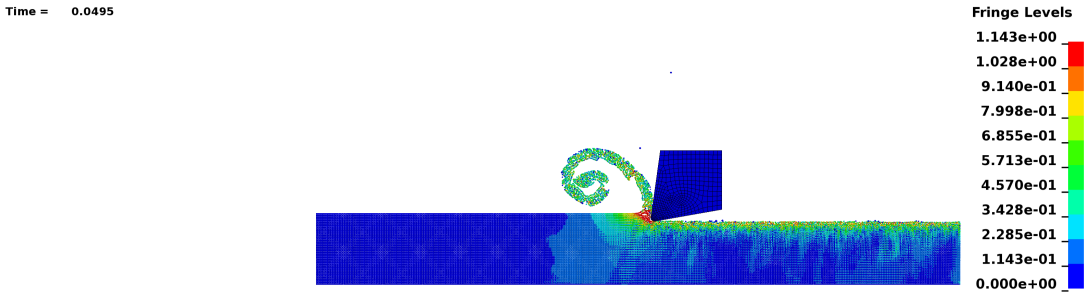

Depth of cut = 0.05 mm.

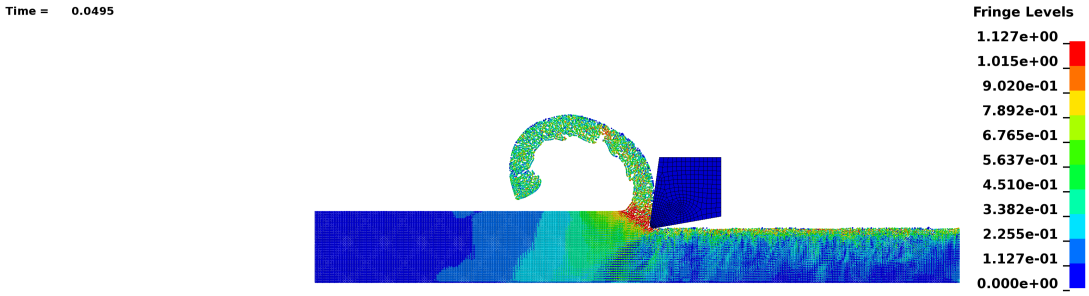

Depth of cut = 0.1 mm.

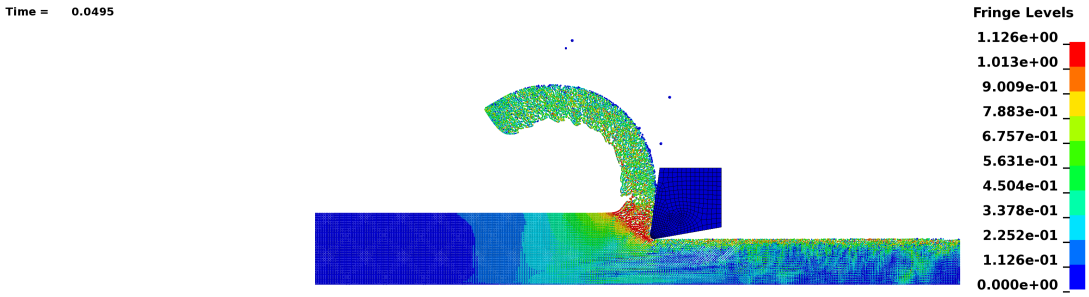

Depth of cut = 0.15 mm.

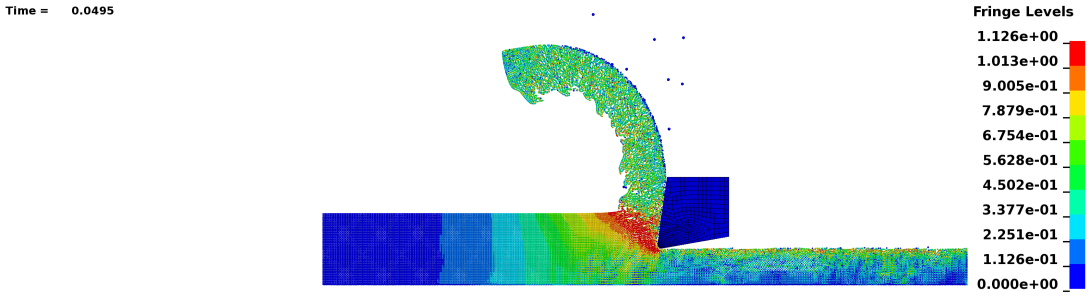

Depth of cut = 0.2 mm.

Figure 5.14: Contour plot of von Mises stress (GPa) for various depths of cut at time $t = 0.0495$ ms.

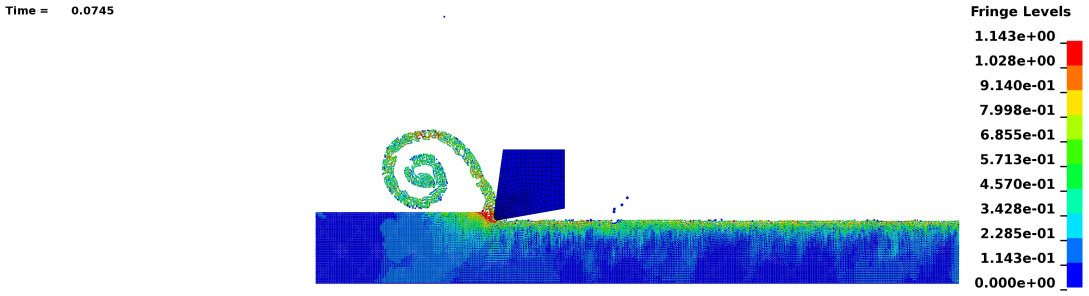

Depth of cut = 0.05 mm.

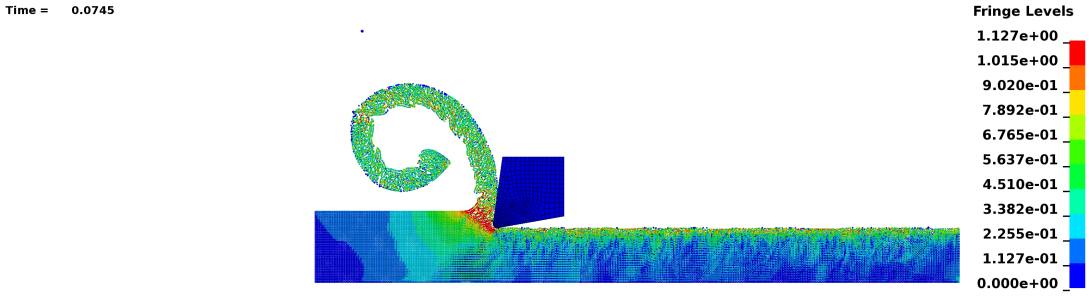

Depth of cut = 0.1 mm.

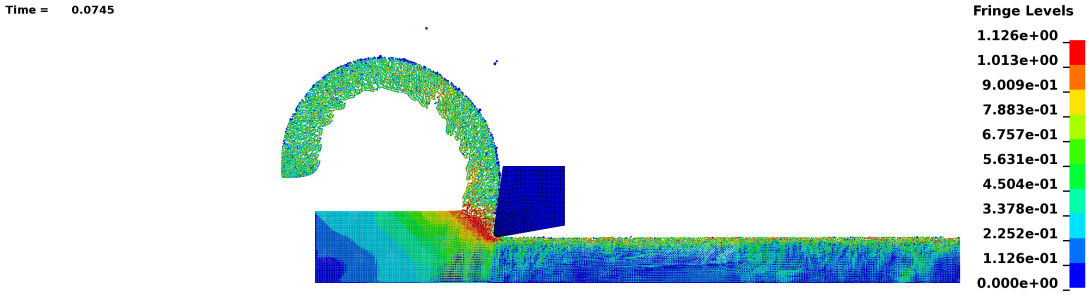

Depth of cut = 0.15 mm.

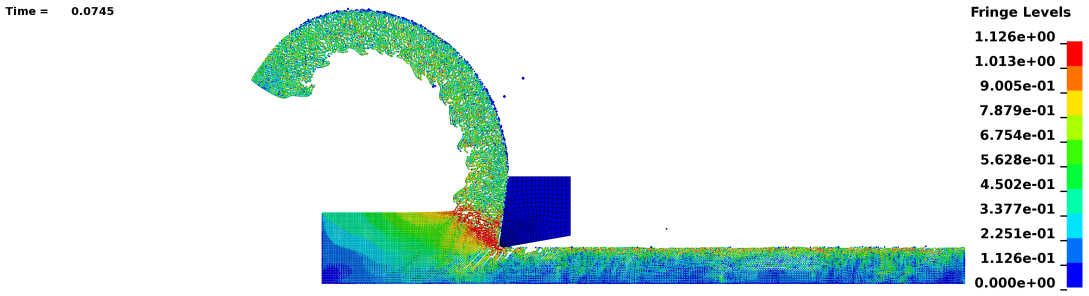

Depth of cut = 0.2 mm.

Figure 5.15: Contour plot of von Mises stress (GPa) for various depths of cut at time $t = 0.0745$ ms.

5.5 Variation of Cutting Speed

To investigate the effect of the cutting speed on the results, a parametric study with different values of cutting speed was conducted. All other parameters were kept the same. It is observed that as the cutting speed is increased, the maximum stress value increases. There are also changes observed with the chip morphology with respect to chip curl radius which increased with increase in cutting speed. Another important observation was that the computation time reduces as the cutting speed is increased, which is in agreement with the literature [26, 28]. The results showing the cases with different cutting speeds at different stages during the simulation are shown in Figures 5.16, 5.17 and 5.18

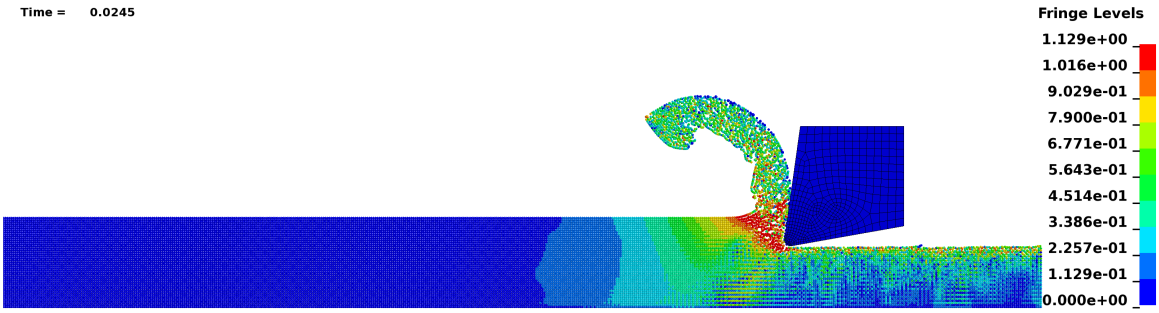

Cutting speed of 2100 m/min with a total simulation time of 0.1 ms.

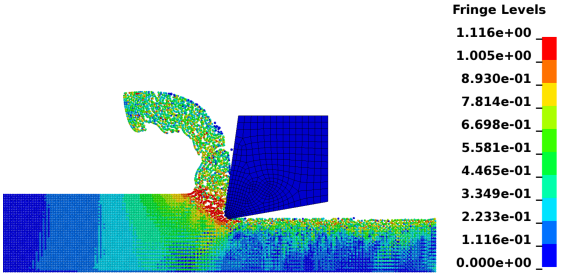

Cutting speed of 500 m/min with a total simulation time of 0.4 ms.

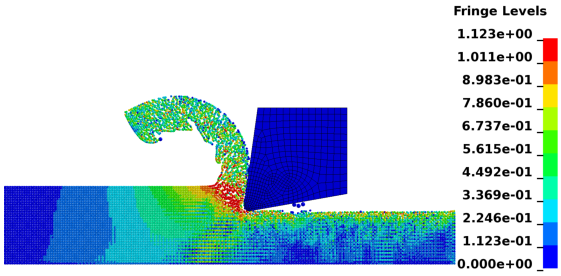

Cutting speed of 1000 m/min with a total simulation time of 0.2 ms.

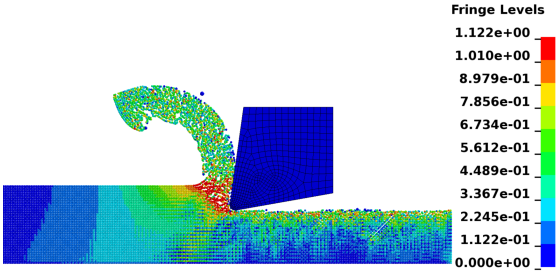

Cutting speed of 1500 m/min with a total simulation time of 0.14 ms.

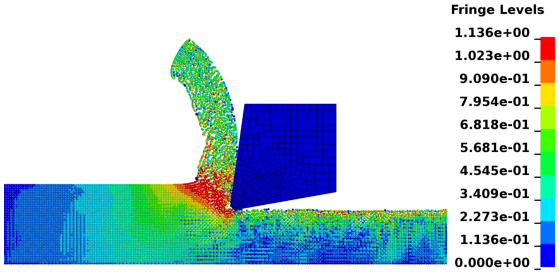

Cutting speed of 5000 m/min with a total simulation time of 0.04 ms.

Figure 5.16: Contour plot of von Mises stress (GPa) for various cutting speeds at 25% completion of the simulation.

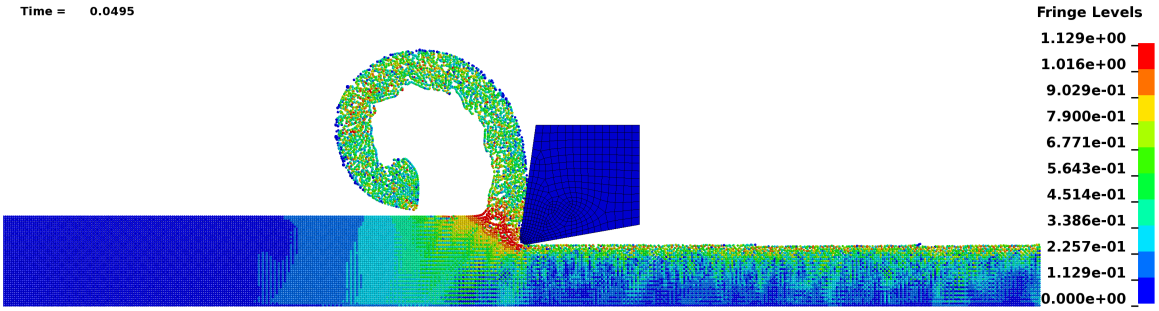

Cutting speed of 2100 m/min with a total simulation time of 0.1 ms.

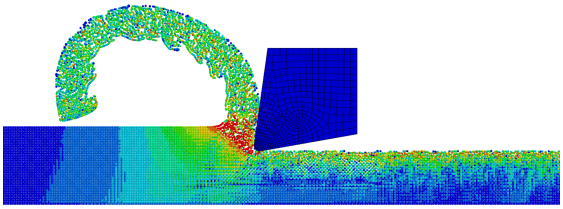

Cutting speed of 500 m/min with a total simulation time of 0.4 ms.

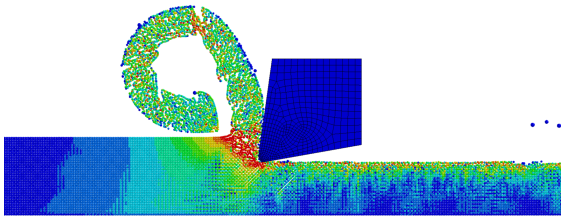

Cutting speed of 1000 m/min with a total simulation time of 0.2 ms.

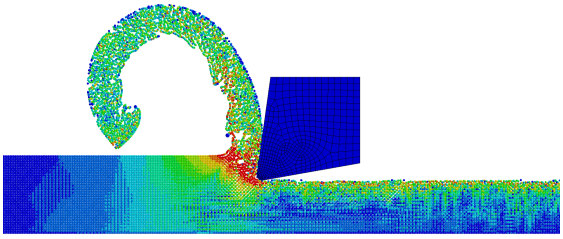

Cutting speed of 1500 m/min with a total simulation time of 0.14 ms.

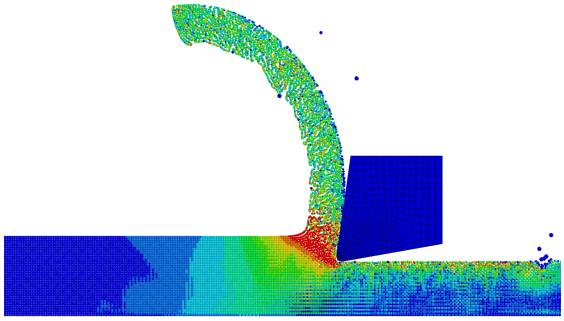

Cutting speed of 5000 m/min with a total simulation time of 0.04 ms.

Figure 5.17: Contour plot of von Mises stress (GPa) for various cutting speeds at 50% completion of the simulation.

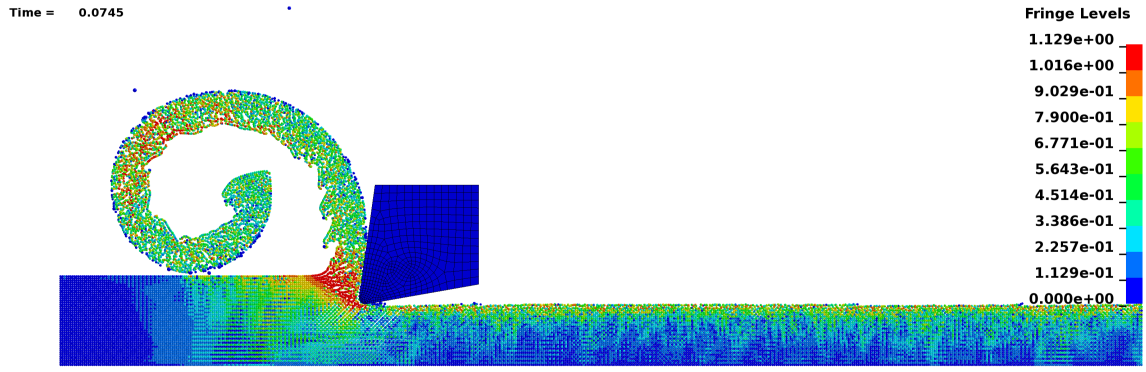

Cutting speed of 2100 m/min with a total simulation time of 0.1 ms.

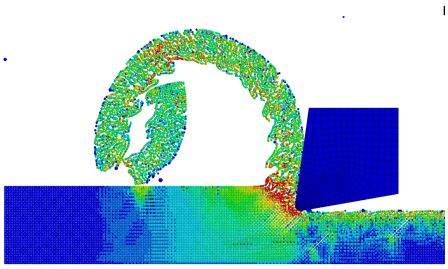

Cutting speed of 500 m/min with a total simulation time of 0.4 ms.

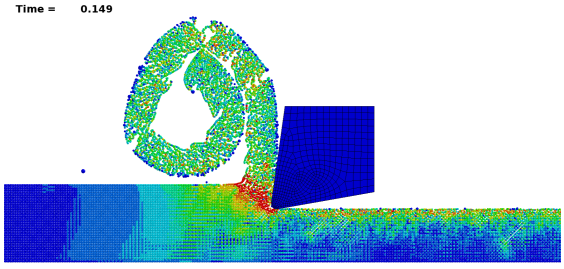

Cutting speed of 1000 m/min with a total simulation time of 0.2 ms.

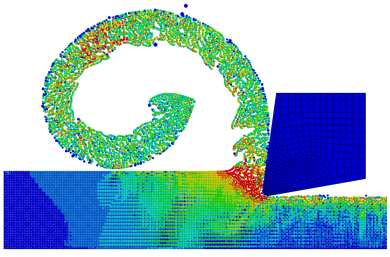

Cutting speed of 1500 m/min with a total simulation time of 0.14 ms.

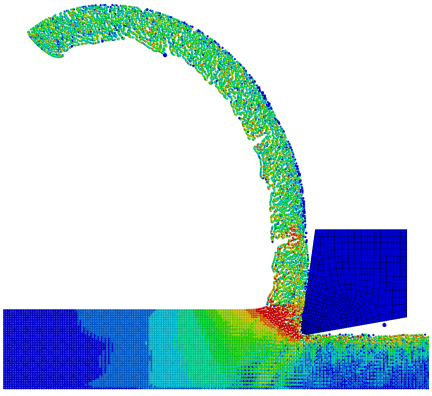

Cutting speed of 5000 m/min with a total simulation time of 0.04 ms.

Figure 5.18: Contour plot of von Mises stress (GPa) for various cutting speeds at 75% completion of the simulation.

CHAPTER 6: CONCLUSIONS

In this study, the smoothed particle hydrodynamics (SPH) method was used to develop an orthogonal machining model for `AISI 1045` steel. The commercial finite element package `LS-DYNA` was used for this purpose. The obtained results were compared with experimental and numerical studies from the literature. The various method for modeling machining such as the analytical methods, numerical methods which include the Lagrangian formulation, Eulerian formulation, arbitrary Lagrangian-Eulerian (ALE) formulation and more importantly the meshfree smoothed particle hydrodynamics formulation were studied. Furthermore, the important aspects of the SPH method such as the kernel function, smoothing length, particle search and also, the pitfalls of the SPH method were studied.

Machining is a complex process to both measure and model and thus, previously conducted research was studied. There are limitation in both experimental techniques as well as modeling the machining process due to various minute phenomena occurring. In spite of this, the numerical models and experimental methods keep achieving higher coherence and accuracy by better understanding the phenomena occurring.

The results obtained from the simulation are in good agreement with experimental and numerical data found in the literature with respect to the von Mises stress, plastic strain and cutting force. The simulated material separation is more natural, especially near the tool-tip. The energy balance diagram showed that the difference between external work and total energy was very low and thus, the simulation was confirmed to be valid. Parametric studies were performed by varying the SPH control parameters.

Particle density was increased to conduct a convergence study. The values of

von Mises stress converged towards the experimental values. The computation time increased as the number of particles were increased.

Simulations with various types of SPH formulation available in `LS-DYNA` were conducted. The adequacy of the renormalization formulation was confirmed and was in agreement with previous studies. The results obtained by using the renormalization formulation show a more physical result.

Cases with different values of the scale factor for computed time-step were simulated. The computation time decreases with increase in the value of the scale factor for computed time-step. Changes were also observed with the chip morphology. The results obtained had good agreement with recent studies.

The importance of using a variable smoothing length in an SPH simulation was investigated and confirmed by reducing the variability of the smoothing length and also simulating cases with a constant smoothing length. Tension instability was observed and resulted in the blowup of the solution when the smoothing length was approximately doubled. Particles were observed to fly out of the domain when a small smoothing length was used as there was less number of initial neighboring particles.

The use of artificial bulk viscosity was found to show a smoother contour plot for von Mises stress. This was coherent with the findings in previous studies.

Johnson-Cook material model parameters obtained from various authors were simulated. The parameters were found to influence the chip morphology as well as field variables such as von Mises stress values.

Cases with various depths of cut were simulated. Except the change in chip morphology, no other significant changes in the results were observed.

The cutting speeds were varied from values between 100 m/min and 5000 m/min and the results obtained showed that as the cutting speed increased, computation time decreased. There were also changes in chip morphology observed with respect to the chip curl radius which increased with the cutting speed.

Finally, it can be concluded from the various studies conducted in this study that the smoothed particle hydrodynamics (SPH) method proves to be a good alternative to conventional finite element methods for modeling orthogonal machining of AISI 1045 steel. There are no problems related to mesh distortions due to large deformation as the SPH method shows a more natural chip-workpiece separation. The SPH orthogonal machining model also showed the self contact that occurs between the curling chip and the workpiece which is not seen with simulations performed using conventional finite element methods. The next step with this capability would be to investigate the friction taking place between this self contact.

With all the merits, there are limitations too, i.e., the physicality and the accuracy of the SPH models are still in question. For instance, thermal contact and conductivity cannot yet be performed in LS-DYNA. A coupled structural-thermal analysis which considers only heat generation inside the SPH workpiece material, does not give physical results as the chip keeps moving upwards and does not curl. Some parameters used to obtain smooth and converging results have totally been obtained through trial and error methods and do not have any physical meaning. Thus, there needs to be further development and investigation into these gray areas. Due to particle sorting and neighbor search the computation times increase significantly.

Provided all the shortcomings are resolved, the SPH method can prove to be a very good alternative to the finite element method to model large deformation processes such as machining as the merits are too attractive to overlook.

REFERENCES

[1] Hallquist, John O. "LS-DYNA theory manual." Livermore Software Technology Corporation 3 (2006).

[2] "ABAQUS Analysis User's Guide,." Dassault Systmes Simulia Corporation (2013).

[3] Childs, Thomas. Metal machining: theory and applications. Butterworth-Heinemann, 2000.

[4] Merchant, M. Eugene. "Mechanics of the metal cutting process. I. Orthogonal cutting and a type 2 chip." Journal of applied physics 16, no. 5 (1945): 267-275.

[5] Merchant, M. Eugene. "Mechanics of the metal cutting process. II. Plasticity conditions in orthogonal cutting." Journal of applied physics 16, no. 6 (1945): 318-324.

[6] Piispanen, Vin. "Theory of formation of metal chips." Journal of Applied Physics 19, no. 10 (1948): 876-881.

[7] Stephenson, David A., and John S. Agapiou. Metal cutting theory and practice. Vol. 68. CRC press, 2005.

[8] Dr. Richard A. Wysk, North Carolina State University, ISE 316: Manufacturing Engineering I; `http://www.ise.ncsu.edu/wysk/courses/ISE316/ISE316-Course-presentation/Ch21.pptx`

[9] Recht, R. F. "Catastrophic thermoplastic shear." Journal of Applied Mechanics 31, no. 2 (1964): 189-193.

[10] Shaw, Milton Clayton. Metal cutting principles. Oxford: Clarendon press, 1984.

[11] Islam, Md Aquidul, "Determination of the Deformation State of a Ti-6Al-4V Alloy Subjected to Orthogonal Cutting Using Experimental and Numerical Methods" (2012). Electronic Theses and Dissertations. Paper 191.

[12] Klamecki, B. E., and S. Kim. "On the plane stress to plane strain transition across the shear zone in metal cutting." Journal of Manufacturing Science and Engineering 110, no. 4 (1988): 322-325.

[13] Carroll III, John T., and John S. Strenkowski. "Finite element models of orthogonal cutting with application to single point diamond turning." International Journal of Mechanical Sciences 30, no. 12 (1988): 899-920.

[14] Shih, Albert J.M., Chandrasekar, S., Yang, Henry T.Y. Finite element simulation of metal cutting process with strain-rate and temperature effects American Society of Mechanical Engineers, Production Engineering Division (Publication) PED, 43 (1990): 11-24.

[15] Komvopoulos, K., and S. A. Erpenbeck. "Finite element modeling of orthogonal metal cutting." Journal of Manufacturing Science and Engineering 113, no. 3 (1991): 253-267.

[16] Zhang, B., and A. Bagchi. "Finite element simulation of chip formation and comparison with machining experiment." Journal of Manufacturing Science and Engineering 116, no. 3 (1994): 289-297.

[17] Marusich, T. D., and M. Ortiz. "A parametric finite element study of orthogonal high-speed machining." In ECCOMAS conference on numerical methods in engineering, pp. 117-131. 1996.

[18] Huang, J. M., and J. T. Black. "An evaluation of chip separation criteria for the FEM simulation of machining." Journal of Manufacturing Science and Engineering 118, no. 4 (1996): 545-554.

[19] Deshayes, Laurent, T. Mabrouki, R. Ivester, and J-F. Rigal. "Serrated chip morphology and comparison with Finite Element simulations." In ASME 2004 International Mechanical Engineering Congress and Exposition, pp. 815-824. American Society of Mechanical Engineers, 2004.

[20] Deshayes, L. "Cutting Methodology Study, Link between Couple Workpiece Tool and Machine Tool Workpiece System (Mthodologie d'tude de la coupe, liaison entre Couple Outil Matire et Pice Outil Machine)." Insa de Lyon (2003).

[21] Buchkremer, S., F. Klocke, and D. Lung. "Analytical study on the relationship between chip geometry and equivalent strain distribution on the free surface of chips in metal cutting." International Journal of Mechanical Sciences (2014).

[22] Bai, Yuanli, and Tomasz Wierzbicki. "Application of extended MohrCoulomb criterion to ductile fracture." International Journal of Fracture 161, no. 1 (2010): 1-20.

[23] Agrawal, Saurabh, and Suhas S. Joshi. "Analytical modelling of residual stresses in orthogonal machining of AISI4340 steel." Journal of Manufacturing Processes 15, no. 1 (2013): 167-179.

[24] Arrazola, P. J., A. Kortabarria, A. Madariaga, J. A. Esnaola, E. Fernandez, C. Cappellini, D. Ulutan, and T. zel. "On the machining induced residual stresses in IN718 nickel-based alloy: Experiments and predictions with finite element simulation." Simulation Modelling Practice and Theory 41 (2014): 87-103.

[25] Heinstein, Martin, and Dan Segalman. "Simulation of orthogonal cutting with smooth particle hydrodynamics." Sandia National Laboratories, California (1997).

[26] Limido, Jrme, Christine Espinosa, Michel Salan, and Jean-Luc Lacome. "SPH method applied to high speed cutting modelling." International journal of mechanical sciences 49, no. 7 (2007): 898-908.

[27] Villumsen, Morten F., and Torben G. Fauerholdt. "Simulation of Metal Cutting using Smooth Particle Hydrodynamics." Tagungsberichtsband zum LS-DYNA Anwenderforum, Bamberg 30, no. 01.10 (2008): 2008.

[28] Espinosa, C., J. L. Lacome, J. Limido, M. Salaun, C. Mabru, and R. Chieragatti. "Modeling high speed machining with the SPH method." In 10th International LS-DYNA Users Conference, Dearborn, Michigan. 2008.

[29] Madaj, Martin, and Miroslav Pka. "On the SPH Orthogonal Cutting Simulation of A2024-T351 Alloy." Procedia CIRP 8 (2013): 151-156.

[30] Heisel, Uwe, Wiliam Zaloga, Dmitrii Krivoruchko, Michael Storchak, and Liubov Goloborodko. "Modelling of orthogonal cutting processes with the method of smoothed particle hydrodynamics." Production Engineering 7, no. 6 (2013): 639-645.

[31] Xi, Yao, Michael Bermingham, Gui Wang, and Matthew Dargusch. "SPH/FE modeling of cutting force and chip formation during thermally assisted machining of Ti6Al4V alloy." Computational Materials Science 84 (2014): 188-197.

[32] Ehmann, K. F., S. G. Kapoor, R. E. DeVor, and I. Lazoglu. "Machining process modeling: a review." Journal of Manufacturing Science and Engineering 119, no. 4B (1997): 655-663.

[33] Markopoulos, Angelos P. Finite element method in machining processes. Springer, 2013.

[34] University of Cambridge, "Analysis of Deformation Processes, Slip Line Field Theory." (2008).

[35] Lee, E. H., and B. W. Shaffer. The theory of plasticity applied to a problem of machining. Division of Applied Mathematics, Brown, 1949.

[36] "The mechanics of machining: an analytical approach to assessing machinability." Ellis Horwood Publisher (1989): 136-182.

[37] Wikiversity, Nonlinear finite elements/Lagrangian and Eulerian descriptions (2010) `http://en.wikiversity.org/wiki/Nonlinear_finite_elements/Lagrangian_and_Eulerian_descriptions`

[38] Mariayyah, Ravishankar. Experimental and numerical studies on ductile regime machining of silicon carbide and silicon nitride. ProQuest, 2007.

[39] Chandrasekaran, Vishnu Vardhan. "Finite element simulation of orthogonal metal cutting using LS Dyna." PhD diss., Auburn University, 2011.

[40] LS-DYNA Examples; Bird Impact on Turbine — `http://www.dynaexamples.com/sph/bird`

[41] Lucy, L. B. "A Numerical Approach to the Testing of Fusion Processes." The Astronomical J 82 (1977): 1013-1024.

[42] Gingold, Robert A., and Joseph J. Monaghan. "Smoothed particle hydrodynamics: theory and application to non-spherical stars." Monthly notices of the royal astronomical society 181, no. 3 (1977): 375-389.

[43] Belytschko, Ted, Yury Krongauz, Daniel Organ, Mark Fleming, and Petr Krysl. "Meshless methods: an overview and recent developments." Computer methods in applied mechanics and engineering 139, no. 1 (1996): 3-47.

[44] Monaghan, Joe J. "Why particle methods work." SIAM Journal on Scientific and Statistical Computing 3, no. 4 (1982): 422-433.

[45] Benz, W. "Smooth particle hydrodynamics: a review." In The numerical modelling of nonlinear stellar pulsations, pp. 269-288. Springer Netherlands, 1990.

[46] Libersky, Larry D., and A. G. Petschek. "Smooth particle hydrodynamics with strength of materials." In Advances in the free-Lagrange method including contributions on adaptive gridding and the smooth particle hydrodynamics method, pp. 248-257. Springer Berlin Heidelberg, 1991.

[47] Allahdadi, Firooz A., Theodore C. Carney, Jim R. Hipp, Larry D. Libersky, and Albert G. Petschek. High strain Lagrangian hydrodynamics: a three dimensional SPH code for dynamic material response. No. PL-TR-92-1054. PHILLIPS LAB KIRTLAND AFB NM, 1993.

[48] Attaway, S. W., M. W. Heinstein, and J. W. Swegle. "Coupling of smooth particle hydrodynamics with the finite element method." Nuclear engineering and design 150, no. 2 (1994): 199-205.

[49] Johnson, Gordon R. "Linking of Lagrangian particle methods to standard finite element methods for high velocity impact computations." Nuclear Engineering and Design 150, no. 2 (1994): 265-274.

[50] Vignjevic, Rade, and James Campbell. "Review of development of the Smooth Particle Hydrodynamics (SPH) method." In Predictive Modeling of Dynamic Processes, pp. 367-396. Springer US, 2009.

[51] Reveles, Juan R. Development of a total Lagrangian SPH code for the simulation of solids under dynamic loading. PhD Thesis. Cranfield University, UK. http://dspace.lib.cranfield.ac.uk/handle/1826/3916

[52] Swegle, J. W., S. W. Attaway, M. W. Heinstein, F. J. Mello, and D. L. Hicks. "An analysis of smoothed particle hydrodynamics." NASA STI/Recon Technical Report N 95 (1994): 17439.

[53] Balsara, Dinshaw S. "Von Neumann stability analysis of smoothed particle hydrodynamicsSuggestions for optimal algorithms." Journal of Computational Physics 121, no. 2 (1995): 357-372.

[54] Johnson, Gordon R., and William H. Cook. "Fracture characteristics of three metals subjected to various strains, strain rates, temperatures and pressures." Engineering fracture mechanics 21, no. 1 (1985): 31-48.

[55] Jaspers, S. P. F. C., and J. H. Dautzenberg. "Material behaviour in conditions similar to metal cutting: flow stress in the primary shear zone." Journal of Materials Processing Technology 122, no. 2 (2002): 322-330.

[56] Liu, Gui-Rong, and Moubin B. Liu. Smoothed particle hydrodynamics: a meshfree particle method. World Scientific, 2003.

[57] KERSHAH, TAREK. "Prediction of cutting coefficients during orthogonal metal cutting process using FEA approach." (2013).

[58] Zouhar, J., and M. Piska. "Modelling the orthogonal machining process using cutting tools with different geometry." MM science Journal (2008): 48-51.

[59] Özel, Tugrul, and Erol Zeren. "Finite element modeling of stresses induced by high speed machining with round edge cutting tools." In ASME 2005 International Mechanical Engineering Congress and Exposition, pp. 1279-1287. American Society of Mechanical Engineers, 2005.

[60] Borkovec, J., and J. Petruska. "Computer simulation of material separation process." Proc. Engineering Mechanics, Svratka, Czech Republic (2007): 14.

[61] Forejt, M. "The mechanical properties of selected types of steel in the condition of higher speed deformation." Report of Research plan MSM 262100003 (2004).

[62] Qian, Li, and Mohammad Robiul Hossan. "Effect on cutting force in turning hardened tool steels with cubic boron nitride inserts." Journal of Materials Processing Technology 191, no. 1 (2007): 274-278.

[63] LACOME, Jean Luc. "Smooth Particle Hydrodynamics (SPH): A new feature in LSDYNA." DYNALIS, Immuable AEROPOLEBat-1 5 (2000).

[64] Fang, Jiannong, Robert G. Owens, Laurent Tacher, and Aurle Parriaux. "A numerical study of the SPH method for simulating transient viscoelastic free surface flows." Journal of non-newtonian fluid mechanics 139, no. 1 (2006): 68-84.